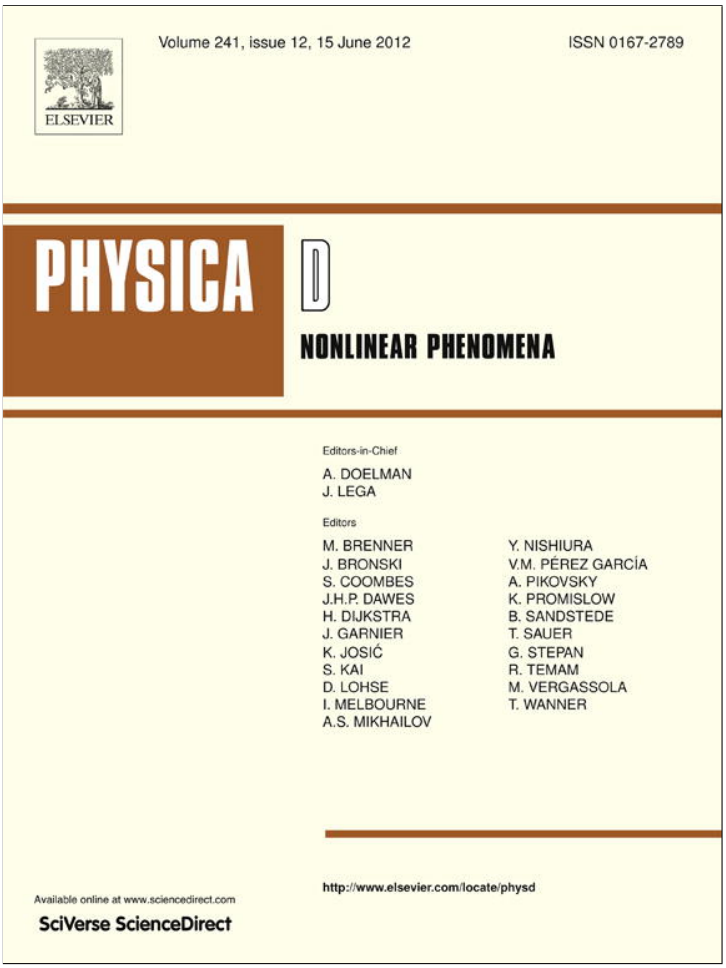

Physica D 241 (2012) 1072–1089

Contents lists available at SciVerse ScienceDirect

Physica D

journal homepage: www.elsevier.com/locate/physd

Bifurcations in phase oscillator networks with a central element

Oleksandr Burylko [a], Yakov Kazanovich [b], Roman Borisyuk [c,b,*]

[a] Institute of Mathematics, National Academy of Sciences of Ukraine, Tereshchenkivska Str. 3, 01601 Kyiv, Ukraine

[b] Institute of Mathematical Problems of Biology, Russian Academy of Sciences, 142290 Pushchino, Russia

[c] School of Computing and Mathematics, University of Plymouth, Plymouth, PL4 8AA, UK

ARTICLE INFO

Article history:
Received 16 May 2011
Received in revised form
22 December 2011
Accepted 29 February 2012
Available online 13 March 2012
Communicated by S. Coombes

Keywords:
Coupled oscillators
Kuramoto model
Networks with a central element
Bifurcations

ABSTRACT

A system of phase oscillators with identical natural frequencies and the star-like architecture of connections is considered. Interaction functions are described by two terms of Fourier expansion. Bifurcation analysis of small systems containing 3 or 4 oscillators has been performed. The results are summarized in bifurcation diagrams that provide a full description of the boundaries between regions with different dynamics and the types of bifurcations that lead to the changes in the topology of phase space. The bifurcations include changes of fixed point stability and formation (destruction) of limit and heteroclinic cycles. For the system with 4 oscillators chaotic behaviour has been investigated. The results can be useful to control system dynamics through an appropriate choice and variation of parameter values. The generalization of the results to the systems with an arbitrary number of oscillators and application of the results in computational neuroscience are discussed.

1. Introduction

Many systems in physics, chemistry and biology can be modelled by coupled phase oscillators of the Kuramoto type [1]. Such models have been found useful for describing dynamics of Josephson-junction arrays, neutrino flavour oscillations, semiconductor laser arrays, coupled magnetic systems, and neural networks. A review of the mathematical theory of phase oscillator networks and their applications can be found in the papers [2,3].

In this paper we consider a special type of phase oscillator networks, the so-called networks with a central element (they are also known as star-coupled networks and can be considered as a special case of networks with the hub structure when a particular part of the network has extensive connections with other parts [3]). In the networks with a central element global interaction is realized through a central oscillator (CO) that has feedforward and feedback connections with all the other oscillators that are called peripheral oscillators (PO). Besides connections with the CO peripheral oscillators may optionally have local connections with their neighbours on a k-dimensional grid.

Networks with a central element appear as parts of more complex networks in so different fields as communication systems, social networks, and mammalian brains. In the latter case they are widely spread due to convergent organization of connections in the hierarchy of brain structures [4,5]. Such networks may play an important role in modelling multisensory integration [6,7] and attention [8,9]. According to Baddeley [10], the attention system is controlled by a central executive, a large-scale network in the frontal cortex. This hypothesis has found an experimental support in a recent work of Gregoriou and co-authors [11]. It has been shown that during visual attention the frontal eye field (an area in the frontal cortex) is a source of increased synchronization at the gamma frequency in the early regions of the visual stream (extrastriate area $V4$). Therefore the study of star-coupled networks can be helpful in clearing up the role of synchronization in cognitive functions. Phase oscillator models provide a convenient and mathematically tractable instrument for this study.

Note that from a biological point of view the networks with a central element are more realistic than those with all-to-all coupling since they demand the number of connections to be of the same order as the number N of elements in the network while for the traditional Kuramoto system the number of connections is N^2. This also facilitates hardware implementation of.star-like architectures.

Though the dynamics of networks with a central element (or their equivalent representation in the form of phase differences, see Eq. (3) below) has been studied in a number of papers [12–20], the detailed bifurcation analysis of such systems is missing with the only exception of networks consisting of Morris–Lecar

* Corresponding author at: School of Computing and Mathematics, University of Plymouth, Plymouth, PL4 8AA, UK.
E-mail address: rborisyuk@plymouth.ac.uk (R. Borisyuk).

0167-2789/$ – see front matter © 2012 Elsevier B.V. All rights reserved.
doi:10.1016/j.physd.2012.02.020

neurons [21]. Here we present such analysis for phase oscillator networks with two and three POs. We restrict the study to the case of oscillators with identical natural frequencies and interaction functions representing two harmonics of the Fourier expansion of a periodic odd function. It will be shown that such interaction functions provide a large variety of stable, oscillatory and chaotic attractors that would be impossible for the sinusoidal interaction function traditionally used in many Kuramoto-like systems. In particular, combining synchronizing and desynchronizing connections it is possible to obtain the competition between the POs for the synchronization with the CO which is important for attention modelling. Also in this case co-existence of different attractors is typical for the network which may be important for modelling perception of ambiguous figures [22].

The results obtained for small systems of phase oscillators can be generalized to the systems with an arbitrary number of oscillators. In this case the complete analysis of bifurcations is hardly possible, but we were able to find the boundaries for some regions with interesting dynamics and to describe several types of local bifurcations such as pitchfork bifurcations, Andronov–Hopf bifurcations, heteroclinic bifurcations of several types, etc. We also present some conditions necessary for chaotic behaviour and its co-existence with attractors of other types.

The boundaries between the regions with different types of dynamics are described in two ways. Some boundaries are described by formulae. These boundaries were derived analytically using standard bifurcation analysis technique [23,24]. For local bifurcations, we worked with eigenvalues of linearized systems. For heteroclinic bifurcations on the phase plane, we used the equality for the saddle quantity of involved saddles, checking also that the eigenvalues for each saddle have opposite signs. Since our analytical methods are routine with a large amount of technical calculations, we did not include these details in the text. Those boundaries that are not described by formulae were computed numerically by using the software package for bifurcation analysis CONTENT (ftp://ftp.cwi.nl/pub/CONTENT). The results of the analysis are shown in the form of bifurcation diagrams with identification of the type of bifurcation that occurs while crossing the boundary between regions in parameter space. The dynamics of the systems are illustrated by numerous examples of phase portraits. The results obtained can be used to control system behaviour by an appropriate selection and variation of system parameters.

2. Model description

We consider a system of one central (CO) and N peripheral (PO) phase oscillators indexed by the numbers $i = 0, \dots, N$. The state of each oscillator is characterized by the phase θ_i ($0 \le \theta_i < 2\pi$). The dynamical equations are assumed to be of the form

$$\begin{aligned} \dot\theta_0 &= \omega_0 + \sum_{j=1}^{N} f_j(\theta_j - \theta_0), \\ \dot\theta_i &= \omega_i + g(\theta_0 - \theta_i), \quad i = 1, \dots, N, \end{aligned} \tag{1}$$

where $(\theta_0, \theta_1, \dots, \theta_N) \in \mathbb{T}^{N+1}$ are phase variables on a $(N+1)$-dimensional torus, ω_i are the natural frequencies of the oscillators, the interaction functions $f_i(x)$ and $g(x)$ are odd 2π-periodic, continuous, and satisfy the conditions

$$g(\pi) = 0, \qquad f_i(\pi) = 0, \quad i = 1, \dots, N. \tag{2}$$

We can reduce (1) to the system in phase differences

$$\dot\varphi_i = \Delta_i - \sum_{j=1}^{N} f_j(\varphi_j) - g(\varphi_i), \quad i = 1, \dots, N, \tag{3}$$

where

$$\varphi_i = \theta_i - \theta_0, \qquad \Delta_i = \omega_i - \omega_0, \quad i = 1, \dots, N.$$

In this paper we consider the case of equal natural frequencies:

$$\omega_i = \omega_0 = \omega, \quad \text{or} \quad \Delta_i = 0, \quad i = 1, \dots, N. \tag{4}$$

The systems of type (3) were also investigated in [12,17,19,20].

Our bifurcation analysis will be presented for interaction functions of the form

$$\begin{aligned} f_i(x) &= a_i(\sin(x) + r\sin(2x)), \\ g(x) &= b(\sin(x) + p\sin(2x)), \end{aligned} \tag{5}$$

where a_i, b, r, p are parameters. Such functions contain up to two harmonics of the Fourier expansion of an odd periodic function. Under conditions (4) and (5) Eq. (3) take the form

$$\dot\varphi_i = -\sum_{j=1}^{N} a_j(\sin(\varphi_j) + r\sin(2\varphi_j)) - b(\sin(\varphi_i) + p\sin(2\varphi_i)),$$
$$i = 1, \dots, N. \tag{6}$$

Below we present the bifurcations analysis of system (6) under the variation of parameters a_i, b, r, p. Stationary points of (6) will be of special interest to us since they represent phase-locked modes of system (1). In particular, if the ith coordinate of a stationary point of (6) is 0, this means that synchronization between the CO and ith PO takes place. The study of (6) gives a number of important dynamical modes including heteroclinic cycles, chaos, and competition of POs for the synchronization with the CO.

2.1. Invariant manifolds

(1) System (3) has m-dimensional invariant manifolds

$$M_m = \{(\varphi_1, \dots, \varphi_N) : \varphi_{k_1} = \varphi_{k_2} = \dots = \varphi_{k_{N-m+1}}\},$$
$$m = 1, \dots, N-1, \tag{7}$$

with possible permutations of indexes of variables φ_i.

The system has $n = n(N, m) = C_N^{m-1} m$-dimensional invariant sets. The line

$$M_1 = \{(\varphi_1, \dots, \varphi_N) : \varphi_1 = \dots = \varphi_N\}$$

is a line of D_N symmetry, where D_N is the dihedral group of an N-sided regular polygon.

In the same way, the system can have l groups of oscillators with d_j, $j = 1, \dots, l$, oscillators in each group, ($d_1 + \dots + d_l = d = N - m + l$) with identical values of phases. Then the dimension of each invariant manifold on the group is $m = N - d + l$ and one of the manifolds can be represented (up to permutations) as

$$M_m = M_m(d_1, \dots, d_l) = \{(\varphi_1, \dots, \varphi_N) : \varphi_1 = \dots = \varphi_{d_1},$$
$$\varphi_{d_1+1} = \dots = \varphi_{d_1+d_2}, \dots, \varphi_{d_{l-1}+1} = \dots = \varphi_{d_{l-1}+d_l}\}, \tag{8}$$

There are n invariant manifolds M_m, where

$$n = n(N, d_1, \dots, d_l) = C_N^{d_1} \cdot C_{N-d_1}^{d_2} \cdot \ \cdots \ \cdot C_{N-\sum_{j=1}^{l-1} d_j}^{d_l},$$

$$\sum_{j=1}^{l} d_j \le N.$$

Fig. 1(a) shows a distribution of 11 oscillators on the circle that corresponds to the invariant manifold $M_4(3, 4, 2, 1)$ on the torus $\mathbb{T}^{11}$ for the original system or on the torus $\mathbb{T}^{10}$ for the reduced system.

(2) Consider a symmetric case:

$$f_i(x) = f_j(x) = f(x), \quad i, j = 1, \dots N.$$

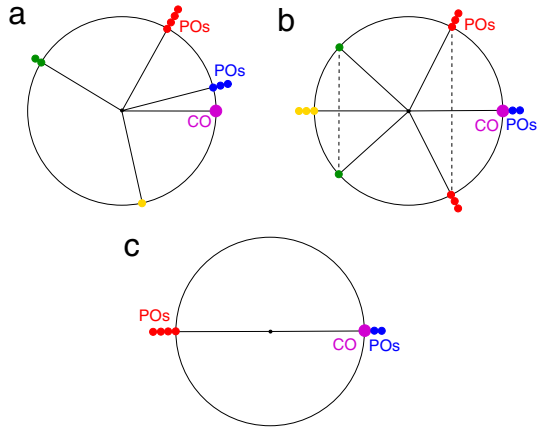

Fig. 1. (Colour online) Examples of oscillators distributed on a circle that correspond to: (a) invariant manifold $M_4(3, 4, 2, 1)$ for 10 peripheral oscillators; (b) invariant manifold Q_2 for 13 peripheral oscillators with symmetries in phase distribution; (c) in-phase and anti-phase synchronization of 6 peripheral oscillators with a CO.

The oddness of the functions $f(x)$ and $g(x)$ implies the conditions:

$$f(\varphi_i)+f(\varphi_j)=0, \qquad g(\varphi_i)+g(\varphi_j)=0, \quad \text{when } \varphi_i+\varphi_j=0 \quad \forall i\neq j=1,\dots,N.$$

Using these properties and condition (2), one can prove that system (3) has m-dimensional invariant manifolds

$$Q_m=\{(\varphi_1,\dots,\varphi_N):\ \varphi_1+\varphi_2=0,\dots,\varphi_{2m-1}+\varphi_{2m}=0,\ \varphi_{2m+1},\dots,\varphi_N\in\{0,\pi\}\}, \tag{9}$$

(up to permutations of any indices of the variables φ_i, $i=1,\dots,N$), where $m=1,\dots,[N/2]$, ($[x]$ denotes integer part of x). There are $n=n(N,m)$ invariant manifolds Q_m in $\mathbb{T}^N$, where

$$n=n(N,m)=2^{N-2m}C_N^{2m}(2m-1)!.$$

Each 1-dimensional invariant line Q_1 is an axis of Z_2 symmetry of system (3). Fig. 1(b) shows a distribution of 14 oscillators that corresponds to the invariant manifold Q_2.

(3) Intersections of 2-dimensional manifolds M_2 with 1-dimensional manifolds Q_1 give 0-dimensional invariant manifolds that represent equilibria Φ^k with k coordinates equal to 0 and $N-k$ coordinates equal to π. Fig. 1(c) shows the distribution of the oscillators that corresponds to the point Φ^2 in $\mathbb{T}^6$. Two of these points $\Phi^N=O=(0,\dots,0)$, $\Phi^0=\Pi=(\pi,\dots,\pi)$ belong to the invariant line M_1. Also we have $n=2^N-2$ other fixed points Φ^k. Note that the intersections of invariant manifolds M_m and Q_l of higher dimensions $m\geq 2$ and $l>1$ create invariant manifolds Q_d ($d<l$). We can also consider all fixed points of the system as 0-dimensional invariant manifolds Q_0 that can be defined by (9) for $m=0$.

2.2. Dynamics on invariant manifolds

Due to the invariant manifolds M_m, system (3) has hierarchical structure. This means that any m-dimensional system (3) has the same dynamics as the dynamics in some invariant manifold (8) of N-dimensional system (3) with new odd functions $\widetilde{f}_i$ that satisfy property (2) ($m<N$). For instance, consider an invariant manifold M_m such that $k_j=j, j=1,\dots,N-m+1$. Then the dynamics inside this manifold satisfy Eq. (3) with new variables

$$\widetilde{\varphi}_1=\varphi_1, \qquad \widetilde{\varphi}_2=\varphi_{N-m+2},\dots,\widetilde{\varphi}_m=\varphi_N$$

and new interaction functions

$$\widetilde{f}_1(\widetilde{\varphi}_1)=\sum_{j=1}^{N-m+1} f_j(\varphi_1),$$

$$\widetilde{f}_2(\widetilde{\varphi}_2)=f_{N-m+2}(\varphi_{N-m+2}),\dots,\widetilde{f}_m(\widetilde{\varphi}_m)=f_N(\varphi_N).$$

In a more complicated case, when we consider system (3) with a number of clusters that correspond to invariant manifolds (8), a system inside an invariant manifold M_m corresponds to the m-dimensional system with new variables that are a part of renumbered old variables and with new interaction functions

$$\widetilde{f}_1(\widetilde{\varphi}_1)=\sum_{j=1}^{d_1} f_j(\varphi_1),$$

$$\widetilde{f}_2(\widetilde{\varphi}_2)=\sum_{j=d_1+1}^{d_1+d_2} f_j(\varphi_{d_1+1}),\dots,\widetilde{f}_l(\widetilde{\varphi}_l)=\sum_{j=d_{l-1}+1}^{d_{l-1}+d_l} f_j(\varphi_{d_{l-1}+1}),$$

$$\widetilde{f}_{l+1}(\widetilde{\varphi}_{l+1})=f(\varphi_{d+1}),\dots,\widetilde{f}_m(\widetilde{\varphi}_m)=f_N(\varphi_N).$$

Thus new functions $\widetilde{f}_i$, $i=1,\dots,m$, in the right side of Eq. (3) are also odd and satisfy the conditions $\widetilde{f}_i(0)=\widetilde{f}_i(\pi)=0$. As we show later, invariant manifolds (8) can have different types of stability in transversal directions depending on variable values inside invariant manifolds and the values of parameters.

Note that Kuramoto-type models of globally coupled oscillators with different coupling functions but with identical natural frequencies do not have such hierarchical structure as our system.

2.3. Symmetries

System (1) has the permutation symmetry S_N of peripheral oscillator phases θ_i, $i=1,\dots,N$. Thus system (3) has S_N symmetry of the variables φ_i, $i=1,\dots,N$. As it was mentioned earlier, the system has D_N-symmetry relative to the axis M_1 and Z_2-symmetry relative to the axes Q_1. It also has S^1 phase shift symmetry:

$$(\theta_0,\theta_1,\dots,\theta_N)\longmapsto(\theta_0+\varepsilon,\theta_1+\varepsilon,\dots,\theta_N+\varepsilon)$$

for any $\varepsilon\in[0,2\pi)$.

In the case of equal parameters $a_i=a, i=1,\dots,N$, system (6) has time-reversed symmetry that can be characterized as actions $\gamma_1,\gamma_2,\gamma_3$ generated by

$$\gamma_1:\ (\varphi_1,\dots,\varphi_N,\ a,\ b,\ p,\ r,\ t)\longmapsto(-\varphi_1,\dots,-\varphi_N,\ a,\ b,\ p,\ r,\ -t)$$

$$\gamma_2:\ (\varphi_1,\dots,\varphi_N,\ a,\ b,\ p,\ r,\ t)\longmapsto(\varphi_1,\dots,\varphi_N,\ -a,\ -b,\ p,\ r,\ -t)$$

$$\gamma_3:\ (\varphi_1,\dots,\varphi_N,\ a,\ b,\ p,\ r,\ t)\longmapsto(\varphi_1+\pi,\dots,\varphi_N+\pi,\ a,\ b,\ -p,\ -r,\ -t).$$

These properties provide the possibility to make conclusions about the dynamics of the system considering only positive (negative) values of parameters.

3. Systems with three oscillators

In this section we consider three coupled oscillators: a central oscillator (CO) and two peripheral oscillators (PO). In this case system (3) in phase differences can be written as

$$\begin{aligned}\dot{\varphi}_1 &= -a_1(\sin(\varphi_1)+r\sin(2\varphi_1))-a_2(\sin(\varphi_2)+r\sin(2\varphi_2))\\ &\quad -b(\sin(\varphi_1)+p\sin(2\varphi_1)),\\ \dot{\varphi}_2 &= -a_1(\sin(\varphi_1)+r\sin(2\varphi_1))-a_2(\sin(\varphi_2)+r\sin(2\varphi_2))\\ &\quad -b(\sin(\varphi_2)+p\sin(2\varphi_2)),\end{aligned} \tag{10}$$

where $\varphi_1=\theta_1-\theta_0$, $\varphi_2=\theta_2-\theta_0$. First we study a symmetrical case of equal coupling strengths of connections from both POs to the CO $a_1=a_2=a$. Since the case $b=0$ is degenerate (only one-way connections from POs to the CO), we assume that $b\neq 0$. Moreover, without loss of generality we set $b=-1$ by scaling the time. Under these conditions we perform the bifurcation analysis of the system in three-dimensional space of parameters (a,p,r).

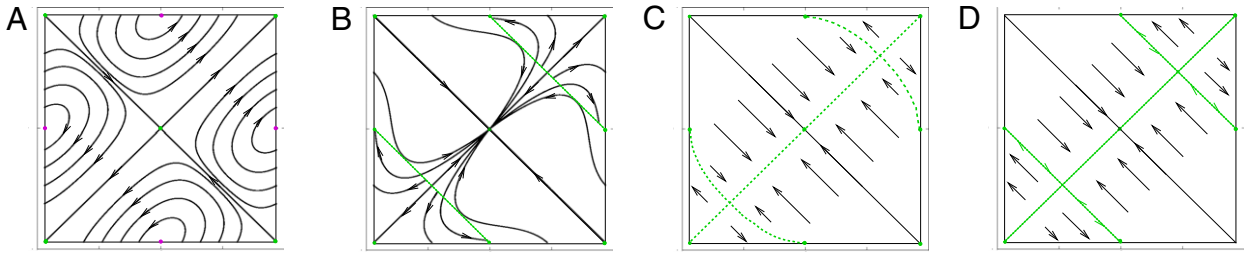

Fig. 2. (Colour online) Phase portraits for $\varphi_1, \varphi_2 \in [0, 2\pi)$, when parameters belong to codimension-2 bifurcation lines (A), (B), (C) in parameter space (a, p, r), and to codimension-3 point (D). Degenerate saddles (with one zero eigenvalue) are shown by dashed green lines.

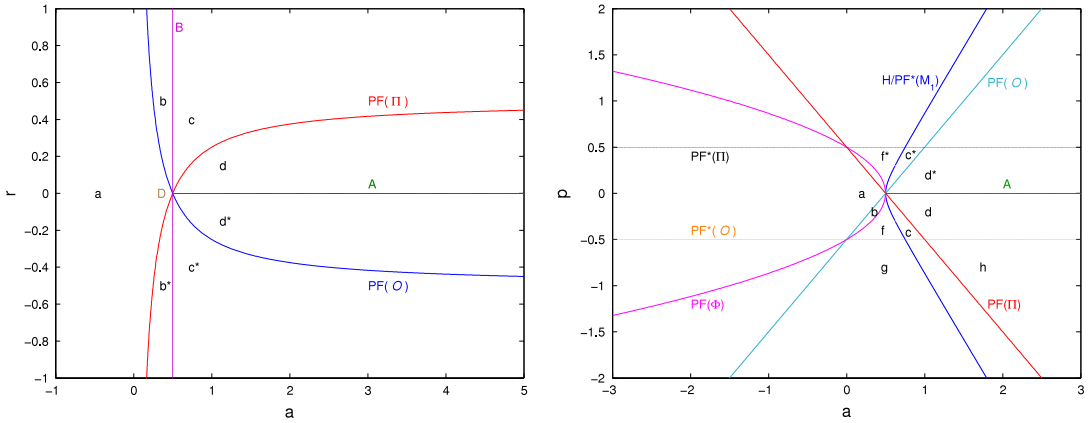

Fig. 3. (Colour online) Bifurcation diagrams on the (a, r) plane for $p = 0$ (left) and on the (a, p) plane for $r = 0$ (right). *PF* and *PF** denote pitchfork bifurcations along invariant lines M_1 and Q_1 correspondingly at the points O, Π, Φ, Φ^*. *A* is a degenerate Andronov–Hopf bifurcation and simultaneously the bifurcation that changes the stability of limit cycles. *B* is a degenerate bifurcation of saddles at Φ, Φ^* and bifurcation of appearance (disappearance) of limit cycles.

Phase space of (10) (the torus $\mathbb{T}^2$) is split into two invariant subspaces by invariant lines

$$M_1 = \{(\varphi_1, \varphi_2) : \ \varphi_1 = \varphi_2\}$$

and

$$Q_1 = \{(\varphi_1, \varphi_2) : \ \varphi_1 = -\varphi_2\}.$$

Also the system has four fixed points $O = (0, 0)$, $\Pi = (\pi, \pi)$, $\Phi = (\pi, 0)$, and $\Phi^* = (0, \pi)$ for any parameter values. Generally speaking, these four points are not the only fixed points of the system, but they can be the only fixed points for some parameter values. The points O and Π can be permuted by the substitution corresponding to the time-reversed symmetry action γ_3. The same is true for the pair Φ, Φ^*. Therefore each of these pairs can be either two saddles (both robust or degenerate) or a source and a sink. If O and Π are robust saddles and if there are no other fixed points on the invariant lines, we obtain a heteroclinic cycle. This cycle can be stable, unstable or neutral depending on the parameters and it can have any of two rotation directions.

It is possible to prove analytically that the system has codimension-1 bifurcation surfaces that are described by the following conditions:

$$\begin{aligned}
&PF^*(O) = \{(a, p, r) : \ p = -1/2\};\\
&PF^*(\Pi) = \{(a, p, r) : \ p = 1/2\};\\
&HC = \{(a, p, r) : \ p = r\};\\
&AH(\Phi) = \{(a, p, r) : \ p = ar\};\\
&PF(O) = \{(a, p, r) : \ p = 2ar + a - 1/2\};\\
&PF(\Pi) = \{(a, p, r) : \ p = 2ar - a + 1/2\};\\
&PF(\Phi) = \{(a, p, r) : \ 8arp - 4p^2 - 2a + 1 = 0\}.
\end{aligned} \tag{11}$$

Note that these three planes, three hyperbolic paraboloids and $PF(\Phi)$ are not the only codimension-1 bifurcation surfaces of the system, but other bifurcation surfaces have more complicated forms. We introduce five lines that play the most important role in system behaviour:

$$\begin{aligned}
&A = \{(a, p, r) : \ a \geq 1/2, \ p = r = 0\},\\
&B = \{(a, p, r) : \ a = 1/2, \ p = 0\},\\
&C = \{(a, p, r) : \ a = 1/2, \ p = r\},\\
&E = \{(a, p, r) : \ p = r = 1/2\},\\
&F = \{(a, p, r) : \ p = r = -1/2\}.
\end{aligned} \tag{12}$$

They are codimension-2 bifurcation lines. Intersections of these lines give codimension-3 points. Let $D = A \cap B \cap C$. Phase portraits corresponding to the cases *A*, *B*, *C*, *D* are shown in Fig. 2.

Almost all of these surfaces represent local bifurcations at equilibria. This allows us to compute the eigenvalues of these points and to find the surfaces (presented above) where these fixed points change their stability. The bifurcation surface *HC* of the heteroclinic bifurcation was found using the equality for the saddle quantity $\rho = 1$ of involved saddles s_j, where $\rho = \rho(s_1, \ldots, s_k) = \prod_{j=1}^{k}(\lambda_-(s_j)/\lambda_+(s_j))$ and the eigenvalues satisfy the inequalities $\lambda_-(s_j) < 0, \lambda_+(s_j) > 0, j = 1, \ldots, k$.

3.1. Description of bifurcations and bifurcation diagrams

In this subsection we describe the dynamics of the system for the cases corresponding to different topologies of phase space (Fig. 4). We present four bifurcation diagrams in three-dimensional parametric space (a, p, r) on the planes: $p = 0$ (Fig. 3 (left)), $r = 0$ (Fig. 3 (right)), $p = r$ (Fig. 7 (left)) and $r = 1/4$ (Fig. 7 (right)). Bifurcation lines of the same bifurcations are presented by the same symbols on each bifurcation diagram (Fig. 3, Fig. 7). The equations of many bifurcation lines are presented in (12) or can be found by a reductions of (11). The dynamics of the system for different parametric regions are marked by different letters. The same letter is used to mark a particular type of dynamics in all

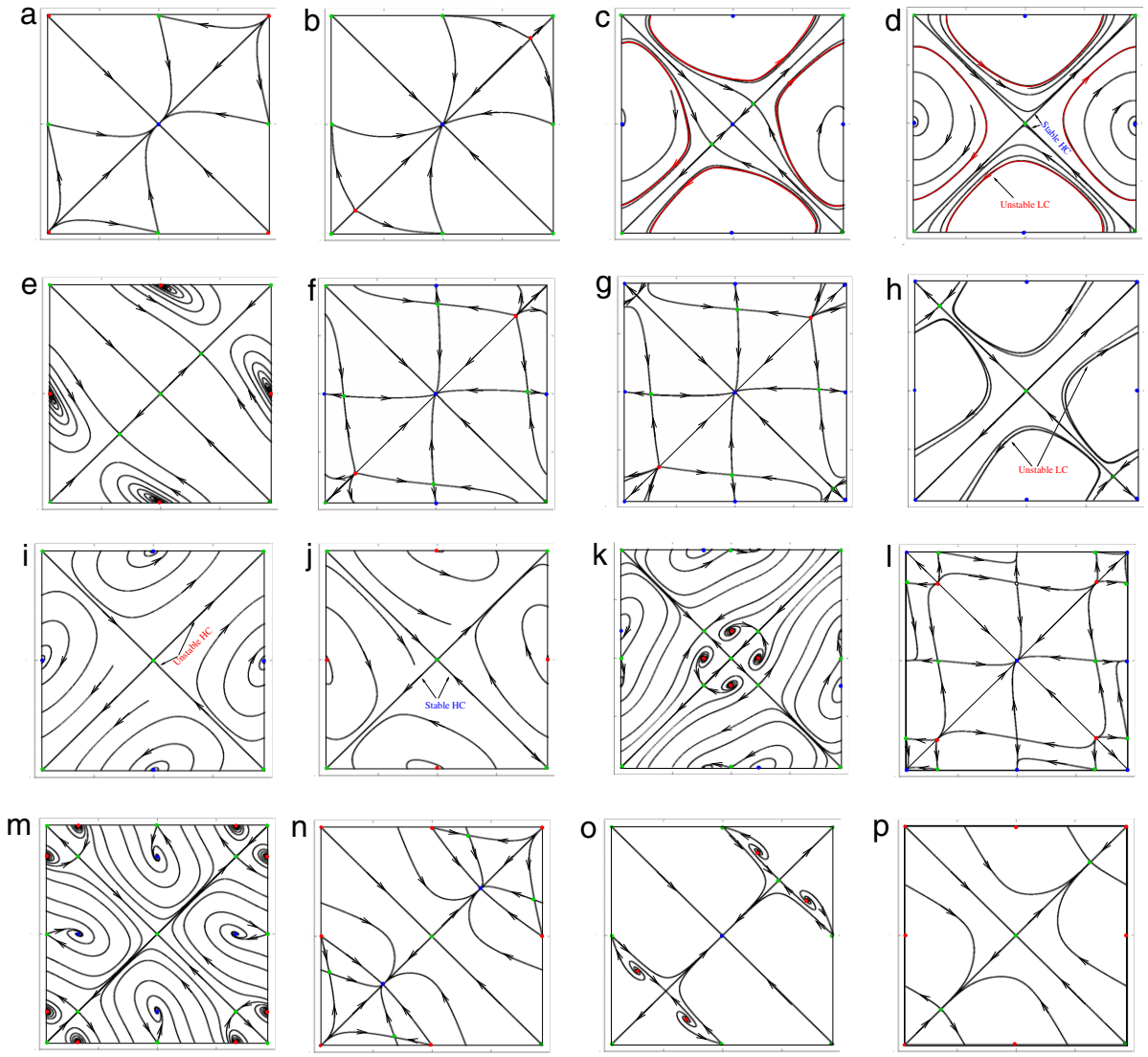

Fig. 4. (Colour online) Phase portraits for $\varphi_1, \varphi_2 \in [0, 2\pi)$. The cases $a, b, c, \ldots, p$ of bifurcation diagrams of Figs. 3, 7, 9 are represented for different values of parameters a, p, r, and for fixed $b = -1$. Some plots of this figure correspond to different bifurcation diagrams. Notation of points: red — source, blue — sink, green — saddle, magenta — saddle–node. Stable limit cycles are shown by blue, unstable by red.

bifurcation diagrams and this letter correspond to the appropriate phase portrait in Fig. 4. The dynamics of the system in the region marked by a letter with a star (for example, b^*) is the same as the dynamics in the region marked by this letter without a star (for example, b) but after applying the time-reversed symmetry action γ_3.

System (10) has the following bifurcations:

(1) $PF(O)$, a pitchfork bifurcation at the origin $O = (0, 0)$ along the invariant line M_1.

(2) $PF(\Pi)$, a pitchfork bifurcation at the point $\Pi = (\pi, \pi)$ along the diagonal M_1.

(3) $PF^*(O)$, a pitchfork bifurcation at the origin along the diagonal Q_1.

(4) $PF^*(\Pi)$, a pitchfork bifurcation at the point Π along the diagonal Q_1.

(5) $PF(\Phi)$, a simultaneous pitchfork bifurcation of the saddles $\Phi = (0, \pi)$ and $\Phi^* = (\pi, 0)$ along their unstable 1-dimensional manifolds.

(6) HC, a homoclinic (heteroclinic) bifurcation of a limit cycle (from inside of the canonical invariant region) and a square heteroclinic cycle (that bounds this region). The limit cycle merges with the heteroclinic cycle and then disappears. Note that the system has two such invariant regions which are bounded by the invariant lines M_1, Q_1 and points O, Π. The eigenvalues at these points satisfy the equality $\lambda_-(O) \cdot \lambda_-(\Pi) = \lambda_+(O) \cdot \lambda_+(\Pi)$, where $\lambda_- < 0$, $\lambda_+ > 0$. The heteroclinic cycles change their stability after the bifurcation.

(7) A, a degenerate Andronov–Hopf bifurcation at the points Φ, Φ^* and simultaneously the bifurcation of stability changing of a limit cycle (the multiplier crosses $+1$). The points Φ, Φ^* are centres at the moment of bifurcation, they are surrounded by a continuous set of concentric periodic trajectories up to the heteroclinic cycle. The heteroclinic cycle consists of two saddle points O, Π and fragments of the diagonals M_1, Q_1. At the moment of bifurcation the heteroclinic cycle changes its stability (Fig. 2(A) and Fig. 4(d), (e)). Thus the line A (Fig. 3, Fig. 7) is a bifurcation line of the "stability shift", where the points Φ, Φ^*, two limit cycles, and the heteroclinic cycle change their stability to the opposite ones.

(8) B, a global bifurcation on the whole line $\mathcal{B} = \{(\varphi_1, \varphi_2) : \varphi_2 = \pm\pi - \varphi_1\}$ of phase space (Fig. 5). Saddles Φ and Φ^* transform into centres (the eigenvalues $\lambda_2 = -\lambda_1 \in \mathbb{R}$ of these saddles meet at the origin and then diverge along the imaginary

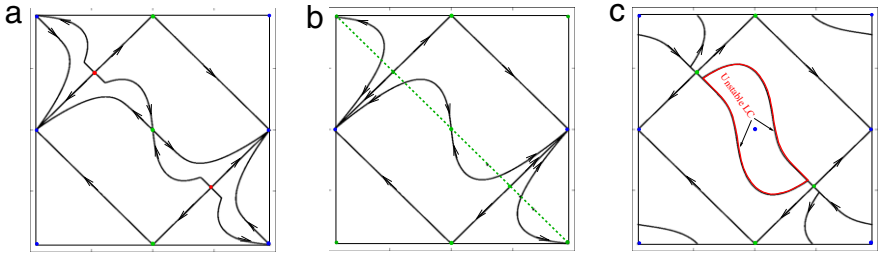

Fig. 5. (Colour online) Phase portraits for $(\varphi_1, \varphi_2) \in [-\pi, \pi) \times [0, 2\pi)$ before (a), at the moment (b), and after the bifurcation on the line **A**.

axis). Sources at the points $(\pi/2, \pi/2)$, $(3\pi/2, 3\pi/2)$ change their stability in the transversal to the diagonal direction. The whole line $\mathcal{B}$ consists of degenerate saddles (with at least one zero eigenvalue) at the moment of the bifurcation (Fig. 5(b)). There are stable and unstable (in the transversal direction) points on the line $\mathcal{B}$. B is also a homoclinic bifurcation which implies the appearance of an unstable limit cycle (Fig. 5(c)).

(9) C, a bifurcation that provides a transition from the case of Fig. 4(a) to the cases of Fig. 4(i) and Fig. 4(j). This bifurcation is represented by the line $a = 1/2$ in Fig. 7 (left). As mentioned above, the line C is a codimension-2 bifurcation line in (a, p, r) parameter space. Two lines of degenerate saddles occur at the moment of bifurcation. One of these lines is the diagonal M_1 and the shape of the other line depends on the parameter r (Fig. 2(C)). The bifurcation changes trajectory directions along the invariant line M_1.

(10) D, codimension-3 bifurcation point in phase space (a, p, r). The lines $\mathcal{B}$ and M_1 consist of degenerate saddles which divide the torus into two parts (Fig. 2(D)). These bifurcation lines separate the regions on the bifurcation diagram (Fig. 3 (left)). The same symbols in the diagrams of Fig. 3 represent the regions with the same (topologically equivalent) dynamics. Phase portraits for the regions are shown in Fig. 4.

(11) NS, neutral saddle bifurcations happen simultaneously at the points O and Π. For each saddle, both eigenvalues are equal to zero at the moment of bifurcation. The bifurcation changes the direction of 1-dimensional invariant manifolds of the saddles. These bifurcations occur simultaneously with $AH(\Phi)$ one the line $a = 1$ when $p = r$ (Fig. 7 (left)).

(12) BT, Bogdanov–Takens bifurcation lines in parametric space (a, p, r) are intersections of $AH(\Phi)$ and $PF(\Phi)$ bifurcation surfaces.

(13) Andronov–Hopf bifurcation connecting two Bogdanov–Takens bifurcations (the brown line connecting two BT points in Fig. 7 (right)). Andronov–Hopf bifurcations happen simultaneously in four symmetrical points (each two of these points appear after a pitchfork bifurcation at the points Φ and Φ^* when the parameter a is decreasing). Two small stable limit cycles appear inside an unstable limit cycle and close to the saddle point Φ. The same happens around another saddle Φ^*.

(14) A symmetric figure-eight shape homoclinic bifurcation of two stable limit cycles that were mentioned in the previous case. A stable limit cycle appears as a result of the described bifurcation. The surface of this bifurcation almost coincides with the surface of the previous bifurcation.

(15) A saddle–node (fold) bifurcation of stable and unstable limit cycles. This bifurcation happens immediately (with parameter changing) after the figure-eight shape homoclinic bifurcation with stable and unstable cycles. Their bifurcation surfaces are also very close to each other. The lines of the last two bifurcations are not shown in the figures.

(16) Homoclinic (saddle-connection) bifurcation of unstable manifolds of the saddles Φ, Φ^* and stable manifolds of the saddles with coordinates $(\pi/2, \pi/2)$ and $(3\pi/2, 3\pi/2)$. The connection lines (1-dimension invariant manifolds of the saddles) are $\varphi_2 = \pm\pi - \varphi_1$. The bifurcation line is $a = 1/2$, $p \in [0, 1/4]$ in Fig. 7 (right).

(17) H/PF$^*(M_1)$, two symmetric pitchfork bifurcations of symmetric saddles $S(\varphi_1, \varphi_1)$ and $S^*(-\varphi_1, -\varphi_1)$ (that belong to M_1) in the transversal M_1 direction create heteroclinic connections (Fig. 3 (right), Fig. 7 (right), Fig. 6). Four points disappear with decreasing $|p|$ and two new limit cycles appear in each invariant region of the torus from heteroclinic cycles. A degenerate saddle that appears at the moment of bifurcation has four saddle regions and one unstable (stable) region.

A large number of codimension-1 bifurcation surfaces in parametric space (a, p, r) create also a lot of bifurcation codimension-2 lines and codimension-3 points. Part of them are mentioned above. As an example, Fig. 7 (right) shows some codimension-2 bifurcation points (intersections of codimension-two bifurcation lines with the parametric plane $(a, p/4, p)$) with coordinates $(0, -1/2)$, $(0, 1/2)$, $(1/2, 0)$, $(1/2, 1/4)$, $(2, -1/2)$, $(2/3, 1/2)$, $(1, 1/4)$, the Bogdanov–Takens point BT (with coordinates approximately equal to $(0.535898, 0.133975)$), and two points of intersection of the line $PF^*(M_1)$ with the lines $PF^*(O)$ and $PF^*(\Pi)$. Note that all bifurcation lines in Fig. 7 (left) are also codimension-2 bifurcation lines in the whole parametric space (a, p, r). Additional symmetry in the case $p = r$ gives additional symmetric pitchfork constructions. For example, the lines E and F present four symmetrical pitchfork bifurcations at the points Π, 0 and a pair of PF bifurcations at the points Φ, Φ^*, which leads to appearance of new fixed points (Fig. 4(k)). It is easy to see that the number of fixed points increases with the increase of parameters $|p|$, $|r|$, but this does not lead to new types of bifurcations.

3.2. Unequal coupling strengths, $a_1 \neq a_2$

Consider system (10) with unequal parameters $a_1 \neq a_2$. The symmetries Z_2 with the centres O, Π, Φ, Φ^* will still exist, but the symmetry D_2 will disappear in the general case and the invariant line Q_1 will be destroyed.

For $a_1 = a_2$ a homoclinic (saddle connection) bifurcation occurs in the case when there are no fixed points on the diagonal Q_1 except O and Π and these two points are saddles. Disconnecting a 1-dimensional invariant manifold from these points leads to disappearance of the (square) heteroclinic cycle (that exists in the symmetric case) and to appearance of a limit cycle with the same stability. Later this cycle can undergo a saddle–node (fold) bifurcation of heteroclinic cycles with the other cycle (that has the opposite type of stability) and then they both disappear (Fig. 8, Fig. 13). In a special case when parameters belong to the line A (the points Φ, Φ^* have neutral stability being surrounded by concentric periodic trajectories), disappearance of the heteroclinic cycle does not lead to appearance of a limit cycle. Also in this case one of the points O or Π becomes a sink and the other one becomes a source, therefore for $a_1 \neq a_2$ there are no periodic trajectories (Fig. 8, Fig. 13).

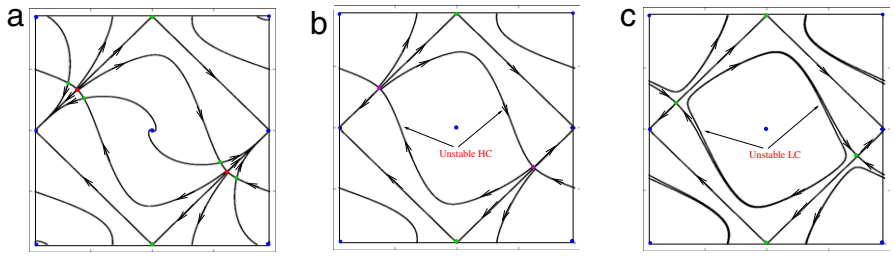

Fig. 6. (Colour online) Phase portraits for $(\varphi_1, \varphi_2) \in [-\pi, \pi) \times [0, 2\pi)$ before homoclinic/pitchfork bifurcation (a), at the bifurcation moment (b), and after bifurcation (c). The bifurcation is depicted by the line H/PF*(M_1) on the bifurcation diagram Fig. 3 (right).

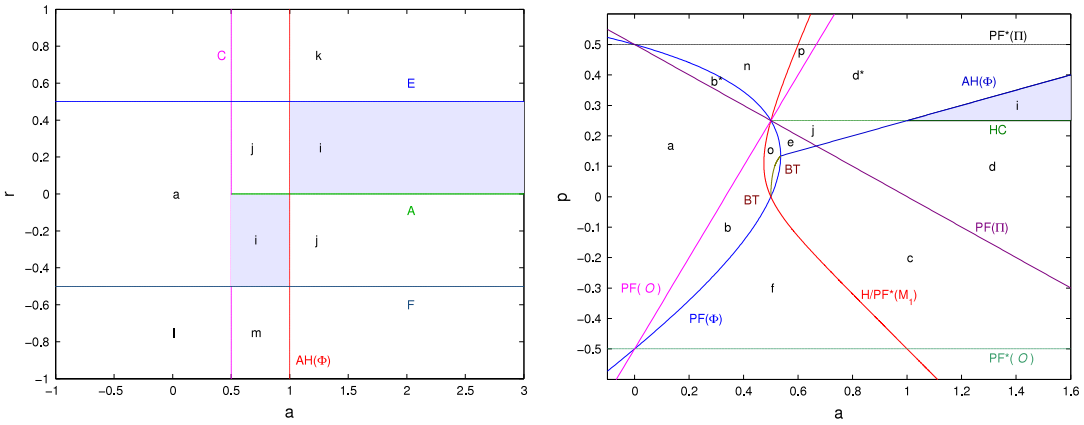

Fig. 7. (Colour online) Bifurcation diagrams on the (a, r) plane for $p = r$ (left) and on the (a, p) plane for $r = 1/4$ (right). Grey regions indicate the cases when the system has just two attractors $(0.\pi)$ and $(\pi, 0)$.

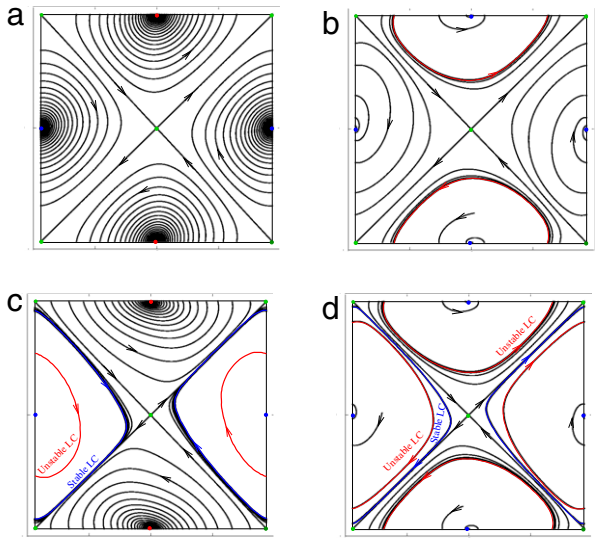

Fig. 8. (Colour online) Phase portraits for $\varphi_1, \varphi_2 \in [0, 2\pi)$ for $a_1 \neq a_2$.

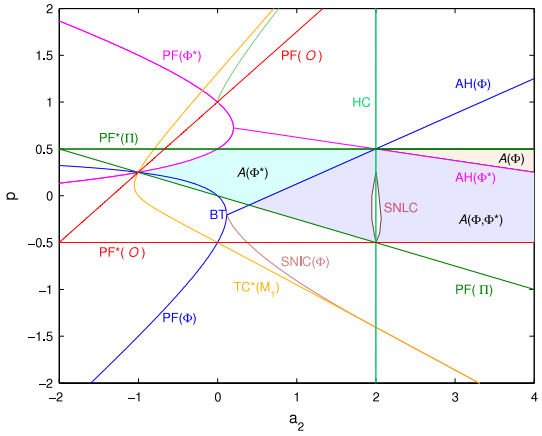

Fig. 9. (Colour online) Bifurcation diagram on the (a_2, p) plane for $a_1 = 2, r = 1/4$.

In the case $a_1 \neq a_2$ the points Φ and Φ^* can have opposite types of stability (this cannot happen if $a_1 = a_2$ due to D_2 symmetry). This means that the CO can synchronize with one PO while being in anti-phase with the other PO. Bifurcation lines for the points Φ and Φ^* are different (Fig. 9) (that would be impossible if $a_1 = a_2$). AH and PF bifurcation lines for the points Φ and Φ^* approach to each other when $a_1 \to a_2$ and merge when $a_1 = a_2$.

Let us consider the bifurcation diagram of Fig. 9 and describe bifurcation lines shown on it:

(1) $PF(O)$, $PF(\Pi)$, pitchfork bifurcations along the invariant manifold M_1 at the points O, Π, respectively.

(2) $PF^*(O)$, $PF^*(\Pi)$, pitchfork bifurcations in the transversal to M_1 direction at the origin and at the point Π, respectively.

(2) $AH(\Phi)$, $AH(\Phi^*)$, Andronov–Hopf bifurcations at the points $(\pi, 0)$ and $(0, \pi)$. The lines of these two bifurcations are different as opposed to the case $a_1 = a_2$.

(3) HC, a homoclinic (heteroclinic) bifurcation of a square heteroclinic cycle that consists of the points O, Π and their stable and unstable 1-dimensional manifolds. The heteroclinic cycles transform into a limit cycle with the same stability $(a_1 \neq a_2)$.

(4) $PF(\Phi)$, $PF(\Phi^*)$, pitchfork bifurcations at the points $(\pi, 0)$ and $(0, \pi)$, respectively.

(5) $TC^*(M_1)$, a transcritical bifurcation of a saddle that belongs to the invariant manifold M_1 with a source in the transversal to M_1 direction.

(6) *SNIC*(Φ), two symmetric saddle–node bifurcations on the invariant cycle that surrounds the point Φ. It is the heteroclinic cycle at the moment of bifurcation that consists of two saddle–node points and two invariant 1-dimensional manifolds.

(7) *SNLC*, two lines of saddle–node (fold) bifurcations of limit cycles. These two lines lie very close to the homoclinic bifurcation line for $a_2 = 2$ and $r \in [-1/2, 1/4]$. Each limit cycle that appears at the moment of homoclinic bifurcation will disappear almost at the same time. Note that the distance between the *SNLC* bifurcation lines enlarges when a_1 is decreasing (this can be seen if we consider the (a_2, p) bifurcation diagram for smaller values of the parameter a_1).

(8) *BT*, a Bogdanov–Takens point that connects *AH*(Φ), *PF*(Φ), and *SNIC*(Φ) bifurcation lines.

Fig. 8 shows the case when the system has only one attractor (Fig. 8(a)), bistability of two points Φ and Φ^* like in the symmetric case (Fig. 8(b)), bistability of a stable point and a cycle (Fig. 8(c)), and multistability of the points Φ, Φ^* and a limit cycle (Fig. 8(d)). All these cases are impossible for $a_1 = a_2$.

In the case when $a_1 = a_2$ we were able to put $b = -1$ and obtain the whole dynamical picture of the system. It is possible to consider a more general system with two different interaction functions $g_1(x)$ and $g_2(x)$ with the parameters of connection strengths b_1 and b_2, respectively. If the parameters a_1 and a_2 are different, we can only fix one of b_i. In this case we could obtain different dynamics for different values of another parameter b_j. This would increase the possibilities for bifurcations of other types, giving new types of heteroclinic cycles and new types of multistability. Note that the system is hamiltonian for $a_i = -b_i$, $p = r$.

3.3. Only two attractors Φ and Φ^*

From a biological point of view a special interest is represented by the case when system (10) has only two attractors at the points $\Phi = (\pi, 0)$ and $\Phi^* = (0, \pi)$. This case corresponds to the synchronization of one of the POs with the CO, while the other PO is in the anti-phase state. This case is important since it represents the competition of POs for the synchronization with the CO.

If $a_1 = a_2$, the points Φ and Φ^* are symmetric relative to the line M_1, therefore they have the same type of stability for any parameter values. Thus we can only have the multistability of these two points (Fig. 4(i)). In this case the system has also a repeller that is a heteroclinic cycle consisting of two saddles O, and Π and their 1-dimensional invariant lines that belong to the diagonals M_1 and Q_1. The heteroclinic cycle consists of four points and four lines if we consider it not on the torus $\mathbb{T}^2$ but on the Euclidean plane $\mathbb{R}^2$. We have two regions $G_1 = \mathcal{A}_1(\Phi)$ and $G_2 = \mathcal{A}_2(\Phi)$ in three-dimensional space (a, p, r) which represent the situation we are interested in. One of them is an infinite domain that is bounded by two planes and a hyperbolic paraboloid:

$$\mathcal{A}_1(\Phi) = \{(a, p, r) : p \geq r,\ p < 1/2,\ p < ar\}.$$

Another region is finite and bounded by a plane and two hyperbolic paraboloids:

$$\mathcal{A}_2(\Phi) = \{(a, p, r) : p \geq r,\ p < ar,\ p < 2ar + a - 1/2\}.$$

Thus the system has two attractors Φ and Φ^* when $(a, p, r) \in \mathcal{A} = \mathcal{A}_1 \cup \mathcal{A}_2$. The intersection of the region $\mathcal{A}$ with the planes $p = r$ and $r = 1/4$ is indicated by grey colour in Fig. 7.

Consider the same problem for the system with $a_1 \neq a_2$. In this situation the system can have three possible types of phase portraits: (1) only one attractor Φ^* (Fig. 8(a)); (2) only one attractor Φ (symmetric to the previous case); (3) bistability of two attractors Φ and Φ^* (Fig. 4(i), and Fig. 8(b)). Three corresponding regions of parameters denoted as $\mathcal{A}(\Phi^*)$, $\mathcal{A}(\Phi)$ and $\mathcal{A}(\Phi, \Phi^*) = \mathcal{A}(\Phi) \cap \mathcal{A}(\Phi^*)$ are shown in Fig. 9.

The region $\mathcal{A}(\Phi, \Phi^*)$ can abruptly enlarge when a_1 differs from a_2. For example, Fig. 9 shows that region $\mathcal{A}(\Phi, \Phi^*)$ occupies the interval $1/4 < p < 1/2$ if $a_1 = a_2 = 2$. But for other values of a_2 even only slightly different from $a_1 = 2$ the region $\mathcal{A}(\Phi, \Phi^*)$ becomes approximately equal to $-1/2 < p < 1/2$ at both sides from the fold bifurcation of limit cycles. Here we can see a typical way of region $\mathcal{A}$ extension when initially stable heteroclinic cycle (that coexisted with the stable points Φ, Φ^*) disappears after a homoclinic bifurcation and transmits its stability to a limit cycle that is born after the bifurcation. Then the new stable limit cycle disappears after the fold bifurcation with an unstable limit cycle. Corresponding phase portraits of this bifurcation transition are shown in Fig. 4(i) and Fig. 8(b), (d).

4. Systems with four oscillators

In this section we consider the model that consists of a CO and three POs. In this case the equations for phase differences take the form

$$\begin{aligned}
\dot\varphi_1 &= -a_1(\sin(\varphi_1) + r\sin(2\varphi_1)) - a_2(\sin(\varphi_2) + r\sin(2\varphi_2)) \\
&\quad - a_3(\sin(\varphi_3) + r\sin(2\varphi_3)) - b(\sin(\varphi_1) + p\sin(2\varphi_1)), \\
\dot\varphi_2 &= -a_1(\sin(\varphi_1) + r\sin(2\varphi_1)) - a_2(\sin(\varphi_2) + r\sin(2\varphi_2)) \\
&\quad - a_3(\sin(\varphi_3) + r\sin(2\varphi_3)) - b(\sin(\varphi_2) + p\sin(2\varphi_2)), \\
\dot\varphi_3 &= -a_1(\sin(\varphi_1) + r\sin(2\varphi_1)) - a_2(\sin(\varphi_2) + r\sin(2\varphi_2)) \\
&\quad - a_3(\sin(\varphi_3) + r\sin(2\varphi_3)) - b(\sin(\varphi_3) + p\sin(2\varphi_3)),
\end{aligned} \tag{13}$$

where $\varphi_1 = \theta_1 - \theta_0$, $\varphi_2 = \theta_2 - \theta_0$, $\varphi_3 = \theta_3 - \theta_0$. As in the previous section, we start from the assumption that all interaction parameters are identical $a_i = a$, $i = 1, 2, 3$, and also put $b = -1$. Under these conditions we perform the bifurcation analysis of the system in parameter space (a, p, r). In contrast to the previous section, the dynamics of the system in three dimensional phase space is much more complicated, in particular chaotic behaviour becomes possible. Then we briefly observe the changes in system dynamics if interaction parameters have different values. Finally the regimes that combine in-phase and anti-phase dynamics between the CO and POs will be described.

4.1. Phase space and invariant manifolds

System (13) has 2-dimensional invariant manifolds (planes)

$$\begin{aligned}
M_2^{(1)} &= \{(\varphi_1, \varphi_2, \varphi_3) :\ \varphi_1 = \varphi_2\}, \\
M_2^{(2)} &= \{(\varphi_1, \varphi_2, \varphi_3) :\ \varphi_1 = \varphi_3\}, \\
M_2^{(3)} &= \{(\varphi_1, \varphi_2, \varphi_3) :\ \varphi_2 = \varphi_3\},
\end{aligned} \tag{14}$$

and a 1-dimensional invariant manifold

$$M_1 = \{(\varphi_1, \varphi_2, \varphi_3) :\ \varphi_1 = \varphi_2 = \varphi_3\} \tag{15}$$

which represents an intersection of planes (14).

Let us assume that $a_1 = a_2 = a_3$. Under this assumption system (13) has additional invariant manifolds

$$\begin{aligned}
Q_1^{(1)} &= \{(\varphi_1, \varphi_2, \varphi_3) :\ \varphi_1 + \varphi_2 = 0,\ \varphi_3 = 0\}, \\
Q_1^{(2)} &= \{(\varphi_1, \varphi_2, \varphi_3) :\ \varphi_1 + \varphi_3 = 0,\ \varphi_2 = 0\}, \\
Q_1^{(3)} &= \{(\varphi_1, \varphi_2, \varphi_3) :\ \varphi_2 + \varphi_3 = 0,\ \varphi_1 = 0\},
\end{aligned} \tag{16}$$

$$\begin{aligned}
Q_1^{(4)} &= \{(\varphi_1, \varphi_2, \varphi_3) :\ \varphi_1 + \varphi_2 = 0,\ \varphi_3 = \pi\}, \\
Q_1^{(5)} &= \{(\varphi_1, \varphi_2, \varphi_3) :\ \varphi_1 + \varphi_3 = 0,\ \varphi_2 = \pi\}, \\
Q_1^{(6)} &= \{(\varphi_1, \varphi_2, \varphi_3) :\ \varphi_2 + \varphi_3 = 0,\ \varphi_1 = \pi\}.
\end{aligned} \tag{17}$$

Each of these manifolds is a line with Z_2 symmetry.

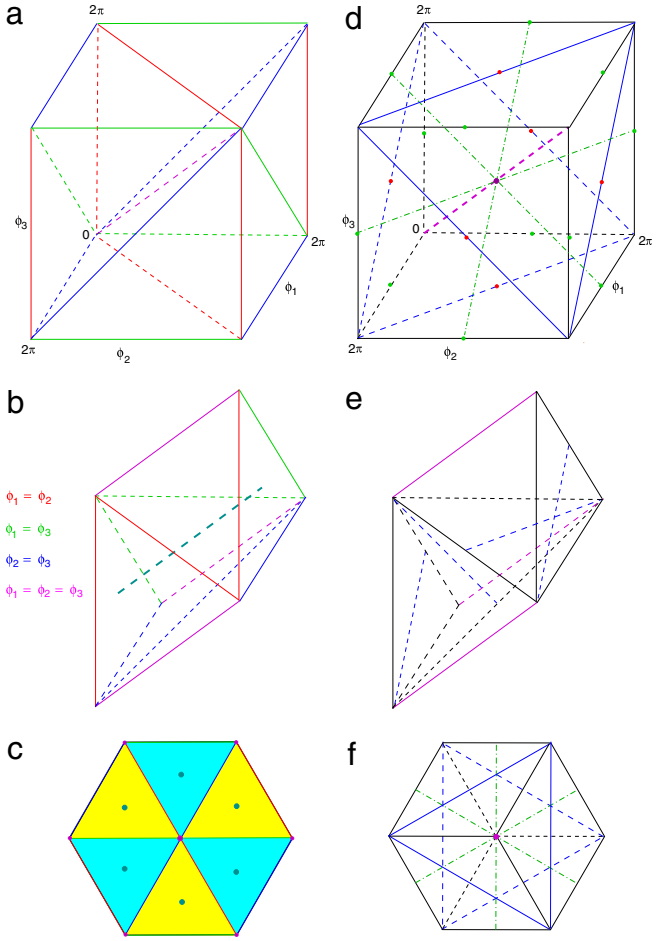

Fig. 10. (Colour online) Schematic diagram for phase space $(\varphi_1, \varphi_2, \varphi_3) \in \mathbb{T}^3$: (a) the cube (torus) with invariant planes $M_2^{(i)}$ (invariant planes are bounded by different colour lines); (b), invariant region bounded by invariant planes; (c) orthogonal projection of the cube on the plane along invariant line (15). (d) invariant lines $Q_1^{(i)}$ inside the cube (torus); (e) invariant lines inside an invariant region; (f) orthogonal projection of invariant lines inside the cube onto the plane along M_1.

Intersections of 1-dimensional and 2-dimensional invariant manifolds create eight 0-dimensional manifolds (fixed points): $O = (0, 0, 0,)$, $\Pi = (\pi, \pi, \pi)$, $\Phi_1 = (0, \pi, \pi)$, $\Phi_2 = (\pi, 0, \pi)$, $\Phi_3 = (\pi, \pi, 0)$, $\Phi_1^* = (\pi, 0, 0)$, $\Phi_2^* = (0, \pi, 0)$, $\Phi_3^* = (0, 0, \pi)$. These 8 fixed points exist for any parameters a, p, r, but for some values of parameters the system can have other equilibria. Each of fixed points mentioned above can change its stability if parameters change their values.

System (13) has permutation symmetry of variables φ_i. Invariant line (15) is an axis of dihedral symmetry D_3 (rotations around the line by the angle $2\pi/3$ and reflections relative to invariant planes (14)). Also each of lines (16), (17) is an axis of Z_2 symmetry (rotations around the line by the angle π) [25].

The invariant planes split the cube into six tetrahedrons (Fig. 10(a)). Each tetrahedron has two closed faces (which are bounded by invariant planes) and two open faces. Thus we can connect tetrahedrons through their open faces obtaining two cases of triangular tubes (Fig. 10(b) shows one of these tubes) that correspond to two invariant regions on the torus $\mathbb{T}^3$. Thereby three invariant planes (14) split the torus into two invariant regions. Each trajectory can locate inside one of the invariant regions but it cannot pass to the other invariant region. An orthogonal projection of the cube along invariant line (15) is shown in Fig. 10(c). In this figure the projections of the same region are shown by the same colour. Thus phase differences between POs are bounded $|\theta_i - \theta_j| < 2\pi$, $i, j = 1, 2, 3$, while a phase difference between the CO and any PO can increase to infinity in R^3. Two types of 1-dimensional invariant manifolds (16), (17) inside the cube (3-dimensional torus) are shown in Fig. 10(d). The invariant lines $Q_1^{(j)}, j = 1, \ldots, 6$, inside an invariant region are shown in Fig. 10(e). The orthogonal projection of the cube along its diagonal and invariant lines mentioned above are shown in Fig. 10(f).

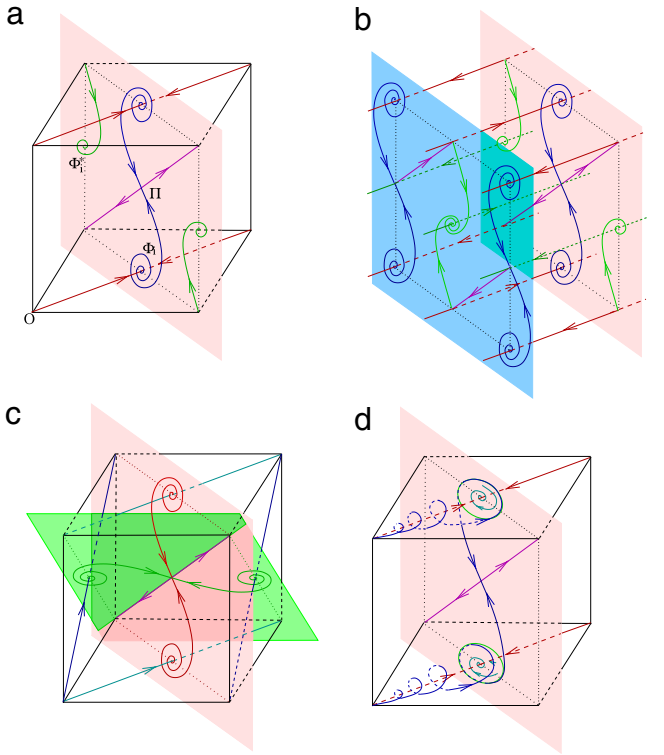

Fig. 11. Schematic diagram for phase space $(\varphi_1, \varphi_2, \varphi_3) \in \mathbb{T}^3$: (a) heteroclinic connection inside the cube (invariant plane and transversal invariant lines); (b) the same invariant plane for two neighbouring cubes and heteroclinic connections; (c) intersection of two invariant planes on the invariant line inside the cube; (d) heteroclinic connection between two points and saddle limit cycles.

Also consider the lines that locate just in the centres of each invariant region:

$$L_1 = \{(\varphi_1, \varphi_2, \varphi_3) : \ \varphi_1 - \varphi_2 = 2\pi/3, \ \varphi_1 - \varphi_3 = 4\pi/3\},$$
$$L_2 = \{(\varphi_1, \varphi_2, \varphi_3) : \ \varphi_1 - \varphi_2 = 4\pi/3, \ \varphi_1 - \varphi_3 = 2\pi/3\}.$$

These lines are shown in Fig. 10(b), (c) (projection). System (13) has the Z_3 symmetry group of rotation around the line L_1 (or L_2) by angle $2\pi/3$ with the simultaneous shift along this line by $2\pi/3$ (rotation around the torus). The lines are not invariant and they intersect $Q_1^{(1)}, \ldots, Q_1^{(6)}$. The system has also another cube rotation symmetry described in [26].

Invariant line (15) connects two points O and Π inside each 2-dimensional invariant plane (14). Also each invariant line (16) connects the point O with each point Φ_i, $i = 1, 2, 3$, which has two coordinates equal to π and the third coordinate 0. These lines connect two different points of the same invariant plane inside the torus T^3 (Fig. 11(b)). In the same way, other three 1-dimensional lines (17) connect the point Π with three different points Φ_i^*, $i = 1, 2, 3$, which have two zero coordinates and one coordinate equal to π. If the point Π is connected with the point Φ_i by some trajectory in the invariant plane, we obtain a closed contour of three points O, Φ_i and Π. This contour can be a heteroclinic cycle $H_3(O, \Phi_i, \Pi) = \{O, W^u(O), \Phi_i, W^u(\Phi_i), \Pi, W^u(\Pi)\}$ when

all its points are saddles and additional conditions $W^u(O) = W^s(\Phi)$, $W^s(\Phi) = W^u(\Pi)$, $W^s(\Pi) = W^u(O)$ are satisfied, where $W^s(x)$, $W^u(x)$ are stable and unstable 1-dimensional manifolds with a starting point x (Fig. 11(a)). Also the heteroclinic cycle $H_3^*(O, \Phi_i^*, \Pi)$ is possible in the system.

More complicated heteroclinic cycles can be constructed combining the previous ones. As an example, the heteroclinic cycle $H_6(O, \Phi_i, \Pi, O, \Phi_i^*, \Pi)$ is shown in (Fig. 11(b)). Note that three different (the same according to symmetry) 3-point heteroclinic cycles have the same part $\{\Pi, W^u(\Pi), O\}$ (Fig. 11(c) shows two such heteroclinic cycles). Heteroclinic cycles $H_6(O, \Phi_i, \Pi, O, \Phi_j, \Pi)$, $i \neq j$, (or even more complicated) are possible as well.

Another example of a heteroclinic cycle is a connection of the saddle points O, Π and a saddle limit cycle that belongs to the invariant plane M_2^i and surrounds the point Φ_i or Φ_i^* (Fig. 11(d)). This heteroclinic cycle appears from $H_3(O, \Phi_i, \Pi)$ (or $H_3(O, \Phi_i^*, \Pi)$) after the Andronov–Hopf bifurcation of the saddle Φ_i (or Φ_i^*). In this way we can obtain a heteroclinic cycle that consists of three saddle limit cycles, points O and Π (which can repeat) and connecting lines.

It can be shown that the origin point is stable along invariant line (16) (more exactly, along the vector $V = (1, -1, 0)$) for arbitrary values of a, r, and $p < -1/2$. The point $(\pi, \pi, 0)$ is stable along the vector V for $p < 1/2$ and arbitrary a, r. Using symmetry we conclude that the point (π, π, π) is stable when $p > 1/2$, and the point $(\pi, 0, 0)$ is stable when $p > -1/2$. Thus a lot of information about dynamics of system (13) can be obtained considering bifurcations on invariant 2-dimensional manifolds (14). Fig. 13 shows phase portraits on the invariant plane $M_2^{(1)}$ for different values of the parameters a and r. Note that bifurcations on the invariant plane are sufficient (but not necessary) conditions for changing qualitative dynamics in the whole 3-dimensional phase space.

4.2. Bifurcations on the planes (a, r) for $p = 0$ and for $p = r$

To describe bifurcations for four coupled oscillators, we consider two cases of parametric planes with varying parameters a, r: $p = 0$ in the first case (Fig. 12 (left)) and $p = r$ in the second one (Fig. 12 (right)). The parameter b is fixed and equal to -1. We present qualitatively different phase portraits on the invariant plane $M_2^{(1)}$ (Fig. 13) since most of the bifurcations (but not all) are two-dimensional. They simultaneously happen inside invariant planes $M_1^{(1)}$, $M_1^{(2)}$, $M_1^{(3)}$ when stabilities in transversal directions do not change. Some of the bifurcations presented on the invariant planes $M_2^{(i)}$ happen in 3D. In particular, bifurcations on the invariant line $M_1 = M_2^{(1)} \cap M_2^{(2)} \cap M_2^{(3)}$ in transversal to this line directions simultaneously happen in three directions in $M_2^{(i)}$.

The system has the following bifurcations:

(1) $AH(\Phi_i)$, a subcritical Andronov–Hopf bifurcation on invariant plane (14) when a saddle-focus point becomes stable and a saddle limit cycle appears in the invariant plane (Fig. 13(a), (b)). The bifurcation line is $r = 1/6$ for $p = 0$ (Fig. 12 (left)).

(2) $AH(\Phi_i^*)$, a supercritical Andronov–Hopf bifurcation on invariant plane (14). The bifurcation line is $r = -1/6$ for $p = 0$ (Fig. 12) (right).

(3) $PF(\Pi)$, a subcritical pitchfork bifurcation at the point Π along invariant line (15) (Fig. 13(b), (c)). The saddle point Π (with two negative and one positive eigenvalues becomes a sink).

(4) $PF(O)$, a supercritical pitchfork bifurcation at O.

(5) $PF^*(\Pi)$, a pitchfork bifurcation at the point Π in 6 directions which gives 12 new points (along the symmetry axes of the cube with the centre in Π). The bifurcation happens for $p = 1/2$.

(6) $PF^*(O)$, a symmetric pitchfork bifurcation at the origin in six directions. Bifurcation plane is $p = -1/2$ for arbitrary r.

(7) $PF(\Phi_i)$, a supercritical pitchfork bifurcation at the points Φ_i, $i = 1, 2, 3$, inside invariant planes (14) (Fig. 13(c), (d)). The sinks (focuses) Φ_i become saddles (with two negative and one positive eigenvalues) and two sinks appear inside each invariant plane (14). The bifurcation line $PF(\Phi_i)$ coincides with line $PF(\Pi)$ in the case $p = r$ and it is $r = 1/2$ in this case.

(8) $PF(\Phi_i^*)$, a subcritical pitchfork bifurcation in Φ_i^*, $i = 1, 2, 3$, inside (14). The line of this bifurcation merges with the line $PF(O)$ for $p = r$, i.e. the surfaces of bifurcations $PF(\Phi_i^*)$ and $PF(O)$ intersect along the line $r = p = -1/2$ in the parametric space (a, p, r).

(9) $AH(M_2)$, a supercritical Andronov–Hopf bifurcation of two points in each invariant 2-dimensional plane (Fig. 13(d), (e)). Each sink becomes a saddle-focus (with a negative real eigenvalue) after the bifurcation.

(10) $AH^*(M_2)$, a subcritical Andronov–Hopf bifurcation of two points in each invariant 2-dimensional plane.

(11) A symmetric figure-eight shape homoclinic bifurcation. This bifurcation happens with two stable limit cycles that appeared earlier after the pitchfork bifurcation of the point Φ_i. The bifurcation implies disappearance of two cycles and appearance of bigger one. The new stable limit cycle is located inside the unstable limit cycles that appeared after the $AH(\Phi_i)$ bifurcation. A similar bifurcation occurs with two unstable limit cycles that appeared after the pitchfork bifurcation at the point Φ_i^* for $r < 0$.

(12) A saddle–node (fold) bifurcation of two limit cycles: the smaller one that appeared after the previous bifurcation and the bigger one that appeared after the bifurcation $AH(\Phi_i)$. Three last bifurcations occur almost simultaneously (transition from the case of Fig. 13(e) to the case of Fig. 13(g)). Thus the bifurcation lines of this and the previous bifurcations are very close to the line $AH(M_2)$, therefore they are not shown on the bifurcation diagram Fig. 12 (left). Note that two similar bifurcations (but with reverse time) occur around the point Φ_i^* for negative values of the parameter r. Their bifurcation lines locate very close to the line $AH^*(M_2)$.

(13) $TC^*(\pi/2)$, a transcritical bifurcation at the point $(\pi/2, \pi/2, \pi/2)$ on each of the invariant planes (14) in the transversal to invariant line (15) direction. The bifurcation line has the equation $a = 1/3$ on the plane $p = 0$. Three saddle-focuses that belong to three different invariant planes $M_2^{(i)}$ meet together at the saddle point S^* with coordinates $(\pi/2, \pi/2, \pi/2)$. This point becomes a source after the bifurcation and three other saddle points S_i leave it. In Fig. 13(g), (h), only projections of these points can be seen on the invariant plane. These figures do not give us full information about qualitative dynamics of the system in 3-dimensional space. In contrast to 2-dimensional space the fixed point S^* changes its stability.

(14) A saddle-connection bifurcation (on the invariant plane) of the unstable manifold of O and stable manifold of the saddle point S_i (Fig. 13(h), (i)). The line of this bifurcation (not shown in the diagram) lies between $TC^*(\pi/2)$ and $PF(\Phi_i^*)$.

(15) Two Bogdanov–Takens bifurcation points for $(a, r) = (1/3, 1/6)$ and $(a, r) = (1/3, -1/6)$ on the bifurcation plane $p = 0$. The lines $AH(\Phi_i)$, $PF(\Phi_i)$, $AH(M_2)$ and also the line of symmetric figure-eight shape homoclinic bifurcations meet at the first BT point. The same happens for Φ_i^* at the second BT-point. Bogdanov–Takens points are presented also on the diagram Fig. 12 (right) for the bifurcation plane $p = r$. The intersection of surfaces $PF(\Phi_i)$ and $AH(M_2)$ creates a codimension-two bifurcation curve of the Bogdanov–Takens bifurcation in (a, p, r)-space.

(16) Codimension-3 bifurcation point $(a, p, r) = (1/3, 0, 0)$ of the intersection of many surfaces. This point is presented on the bifurcation diagram of Fig. 12 (left) for $p = 0$.

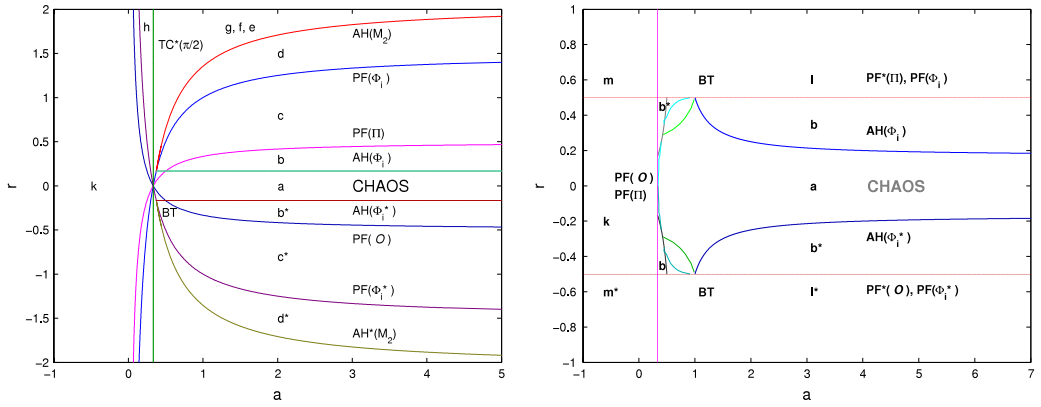

Fig. 12. (Colour online) Bifurcation diagrams on the plane (a, r) for $b = -1$, $p = 0$ (left) and for $p = r$ (right).

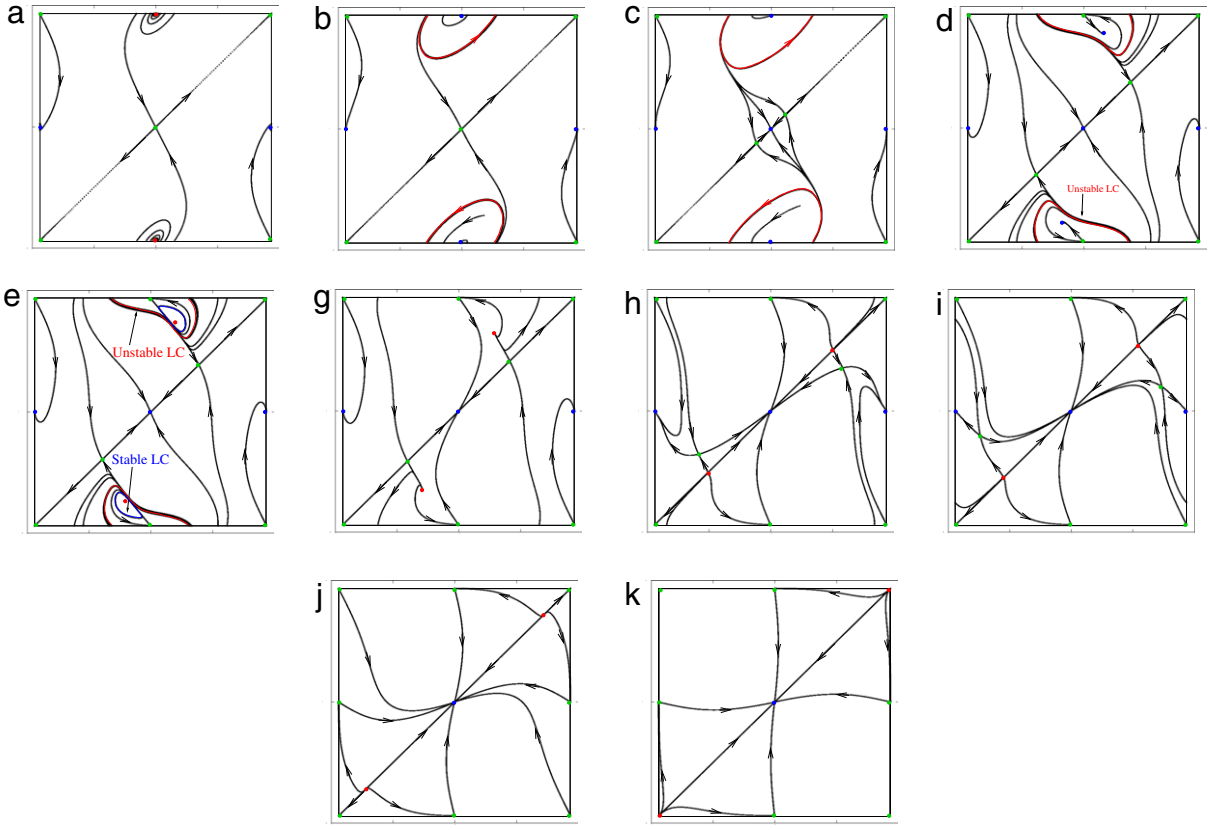

Fig. 13. (Colour online) Phase portraits on the invariant plane $(\varphi_1 = \varphi_2, \varphi_3)$. $b = -1$, $p = 0$.

Remark 1. All 2-dimensional bifurcations that happen around the fixed point Φ_i on the invariant plane $M_2^{(i)}$ (Fig. 13(a), (b), (d)–(g)) are described in [23] p. 426 (cases 1–6, reverse time) and [27] p. 408.

Remark 2. A 2-dimensional system that describes dynamics on invariant plane (14) duplicates the system with three coupled oscillators (CO + 2PO) for $a_1 = 2a_2$ (or $a_2 = 2a_1$).

4.3. Chaos

To understand the chaotic behaviour of system (13), we make a link between (13) and the well known ABC flow (named after Arnold, Beltrami, and Childress, first investigated by Arnold [28]). Consider a system

$$\begin{aligned} \dot\varphi_1 &= A\sin(\varphi_3) + C\cos(\varphi_2 - \delta),\\ \dot\varphi_2 &= B\sin(\varphi_1) + A\cos(\varphi_3 - \delta),\\ \dot\varphi_3 &= C\sin(\varphi_2) + B\cos(\varphi_1 - \delta). \end{aligned} \tag{18}$$

System (18) becomes the ABC flow with parameters A, B, C for $\delta = 0$ and it coincides with Eq. (13) for $a = -b = 1$, $p = r = 0$, when $A = B = C = -1$, $\delta = \pi/2$. The chaotic behaviour of the ABC flow has been studied and described in the literature from different points of view (see [26,28–35]). One can expect that system (13) will show similar behaviour at least for the parameter values mentioned above.

System (18) has eight fixed points (saddles and saddle-focuses) for any value of the parameter δ. There are four α-type fixed points (notation from [31]) with a two-dimensional stable invariant manifold and four β-type fixed points with a two-dimensional

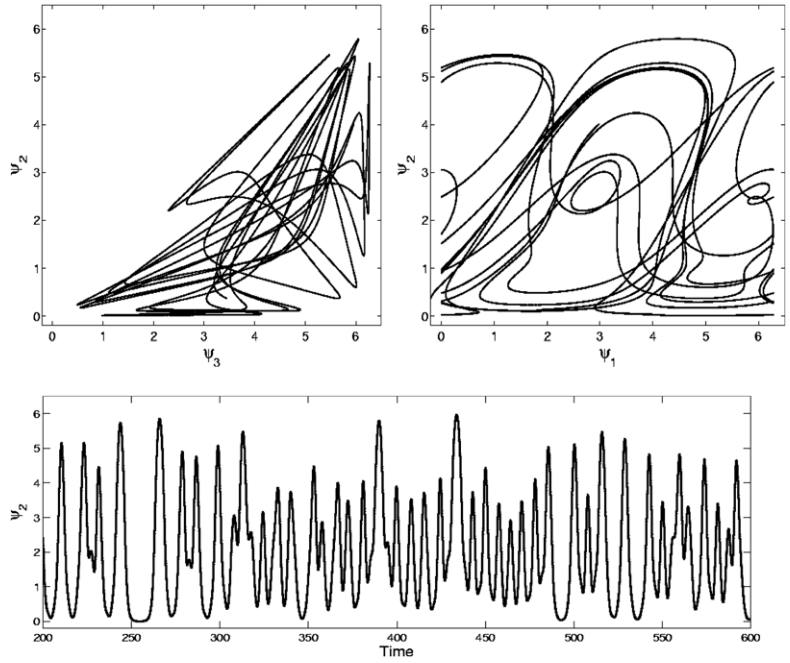

Fig. 14. An example of chaotic trajectory in alternative phase difference variables $\psi_1 = \theta_0 - \theta_1$, $\psi_2 = \theta_2 - \theta_1$, $\psi_3 = \theta_3 - \theta_1$ for $a = -b = 1$, $p = r = 0$.

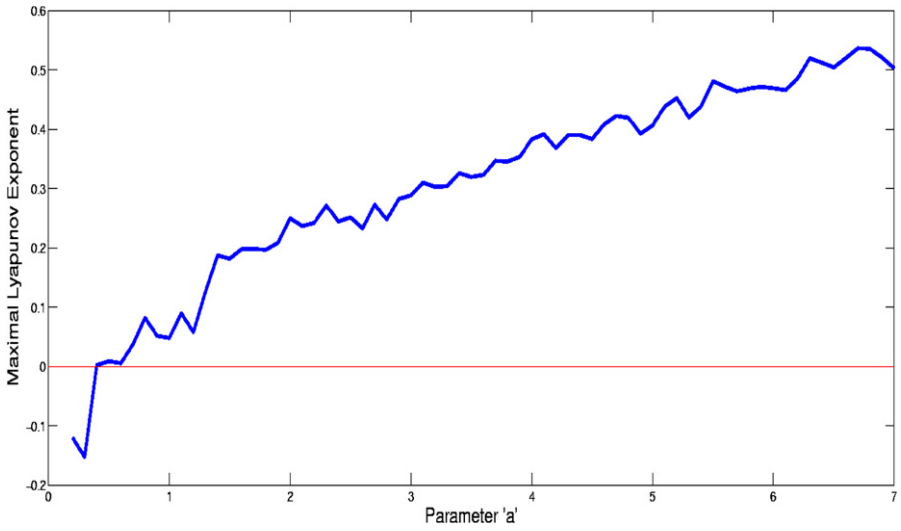

Fig. 15. Maximal Lyapunov exponent versus parameter a for $b = -1$, $p = r = 0.1$.

unstable invariant manifold. It is proved in [36] that fixed points of different types are connected by heteroclinic trajectories for $\delta = 0$. The same situation takes place for (13) (see Fig. 11). One can see that this structure is possible for any value of the parameter δ in (18). A complicated web of heteroclinic connections in the ABC flow appears as a result of intersection of wrapping two-dimensional manifolds of α-type and β-type fixed points [31] (infinitely many heteroclinic lines). This structure causes chaotic behaviour in the system [31]. We conjecture the same nature of chaos in the case $\delta \neq 0$. An example of a chaotic trajectory is shown in Fig. 14.

Consider the situation when the parameters a, p, r are slightly changed in (13). The system has the dynamics that are similar to the previous case. The trajectories pass inside invariant regions (triangular tubes) in two different directions along L_1, L_2 and rotate around each of the invariant lines $Q_1^{(1)}, \ldots, Q_1^{(6)}$. It is impossible to predict how many rotations a trajectory makes around any $Q_1^{(j)}$ and where it goes after that. In contrast to the ABC flow, system (13) has (in a general case) a nonzero divergence. Therefore, the chaotic attractor shrinks around the line L_1 (or L_2) when the parameter a is increasing. Another difference between ABC flows and (13) is that the eigenvalues of the fixed points that belong to the invariant manifolds $M_2^{(i)}$ have imaginary components, i.e. these fixed points are saddle focuses. Variations of the parameters p and r lead to the Andronov–Hopf bifurcation in invariant planes (Fig. 13), appearance of sinks and sources in $\mathbb{T}^3$ and, as a result, disappearance of direct or reverse chaos. Pitchfork bifurcations $PF(O)$ and $PF(\Pi)$ also lead to disappearance of heteroclinic connections and to chaos destruction. System (13) can have two-directional chaos (when the system has chaotic trajectories both for $t \to +\infty$ and $t \to -\infty$). Such dynamics take place when the system parameters belong to the region a in Fig. 12. The regions with one-directional chaos ($t \to -\infty$ or $t \to +\infty$) are marked here by b and b^*, respectively.

Fig. 15 presents a numerical confirmation of the existence of chaos in agreement with the parameter diagram (Fig. 12 (right)).

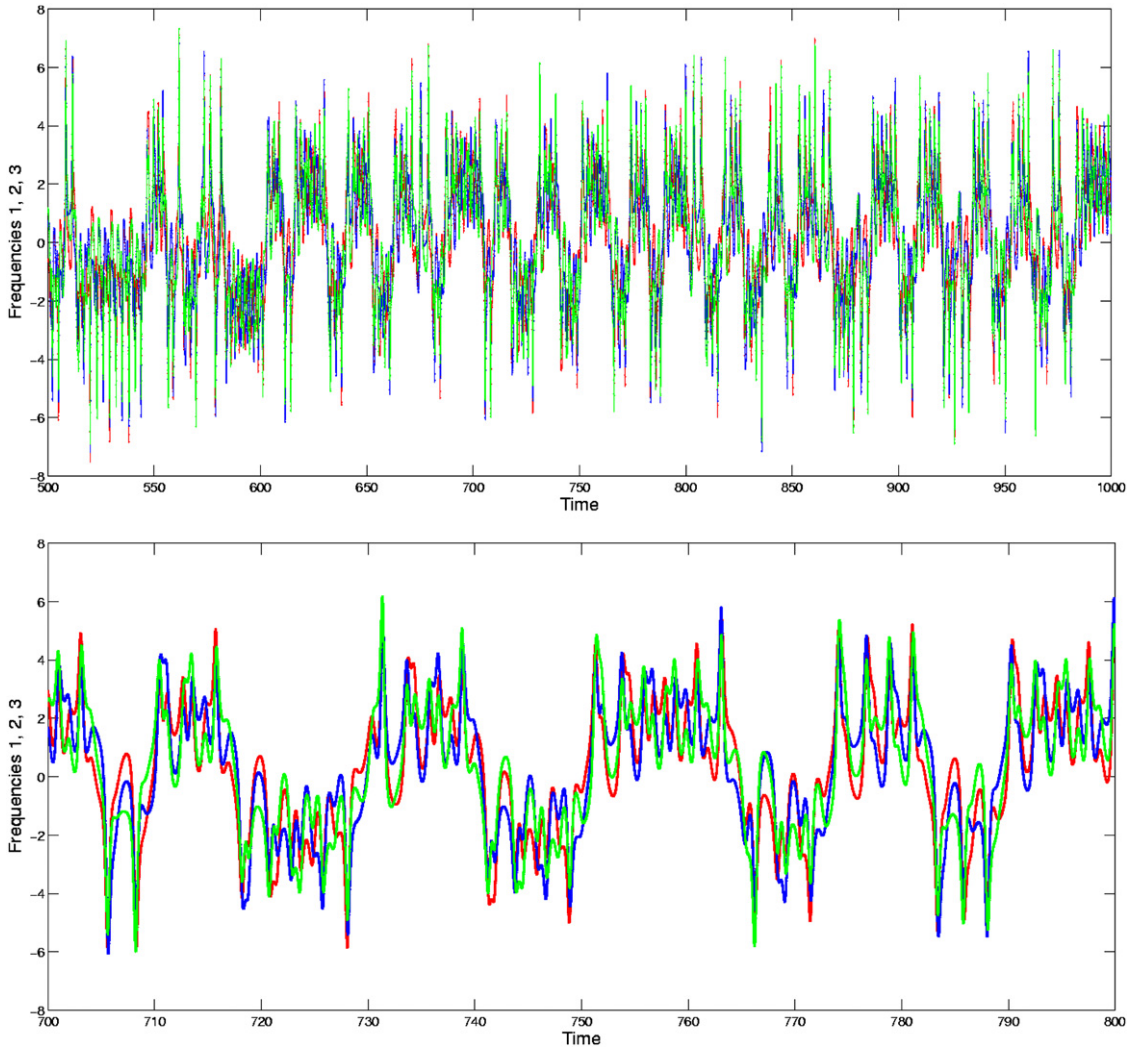

Fig. 16. (Colour online) Frequencies $\dot{\varphi}_1$, $\dot{\varphi}_2$ and $\dot{\varphi}_3$ for $a = 3.5$, $b = -1$, $p = r = 0.1$.

It shows the dependence of the maximal Lyapunov exponent (MLE) on the parameter a. MLE becomes positive for some values of $a > 1/3$. The behaviour of three frequencies $\dot{\varphi}_1$, $\dot{\varphi}_2$, $\dot{\varphi}_3$ corresponding to chaotic dynamics of system (13) is shown in (Fig. 16).

4.4. Unequal coupling strengths

Consider the case when the parameters a_i, $i = 1, 2, 3$, have different values. Planes (14) are still invariant in this case (this means that two triangular invariant tubes still exist), but invariant lines (16), (17) are now destroyed by saddle connection bifurcations. There are no connections $O\Phi_i$ or $\Phi_i^*\Pi$ anymore. Disappearance of these lines destroys heteroclinic connections that were present in the symmetric case (Fig. 11) but new asymmetric heteroclinic connections appear between saddle points. The system still has chaotic attractors which can coexist with other stable solutions.

As we have noted, the points Φ_i (Φ_i^*), $i = 1, 2, 3$, are equivalent under the permutation symmetry if $a_1 = a_2 = a_3$. Thus the system has the same bifurcation lines (which are usually Andronov–Hopf or pitchfork bifurcation lines) for Φ_i (Φ_i^*). The situation is completely different when a_i are unequal. The fixed points Φ_i and Φ_i^*, $i = 1, 2, 3$, have different types of stability. As a result, the system has different bifurcation lines for each of six points mentioned above. Fig. 17 represents a partial bifurcation diagram in this case. We fix the parameters $a_1 = 1$, $a_2 = 1.5$, and $r = 0.25$ and vary the parameters a_3 and p. The diagram does not describe the symmetric case $a_1 = a_2 = a_3$ but shows partially symmetric cases $a_1 = a_3 = 1$ and $a_2 = a_3 = 1.5$, where the homoclinic bifurcations HC_1, HC_2 happen on lines (16), (17) in phase space. We mark the Andronov–Hopf bifurcation at the points Φ_i, Φ_i^* by AH_i, AH_i^*, $i = 1, 2, 3$. The pitchfork bifurcations at these six points are denoted here as $PF(\Phi_i)$ and $PF(\Phi_i^*)$.

Note that PF bifurcations for some points consist of two parts. The points O and Π have a pitchfork bifurcation along the invariant line M_1 and in the transversal to this line direction. The corresponding bifurcation lines are marked as $PF(O)$, $PF(\Pi)$ and $PF^*(O)$, $PF^*(\Pi)$, respectively. The transcritical bifurcation $TC^*(M_1)$ occurs on the invariant line M_1 in the transversal to this line direction. The system has some bifurcation lines that are not shown in Fig. 17. These are saddle–node bifurcations on invariant cycles (the lines start from the points of a Bogdanov–Takens bifurcation that are intersections $BT_i = AH_i \cap PF(\Phi_i)$, $BT_i^* = AH_i^* \cap PF(\Phi_i^*)$), figure-eight shape homoclinic bifurcations, and some bifurcations that lead to chaos. The point U with coordinates $(-3/2, 1/4)$ is an intersection of pitchfork bifurcation lines and three Andronov–Hopf bifurcation lines. All these bifurcations occur simultaneously at five different points. This situation is similar to the one that happens with two POs (Fig. 2(c)). The whole invariant line M_1 consists of degenerate points (with zero eigenvalues) and there are three other lines in phase space that consist completely of degenerate points. Stabilities (in the transversal directions) of the points on these four lines are different.

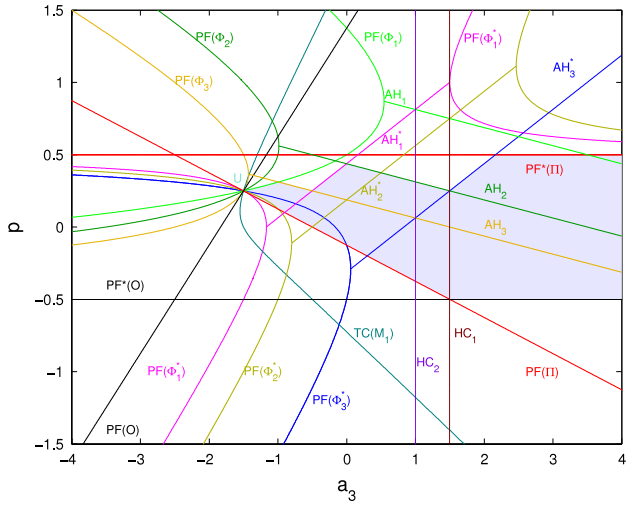

Fig. 17. (Colour online) Partial bifurcation diagram on the plane (a_3, p) for $b = -1$, $r = 0.25$, $a_1 = 1$, $a_2 = 1.5$.

4.5. The points Φ_i and Φ_i^* are the only attractors of the system

The points Φ_i correspond to in-phase synchronization of one PO with the CO and anti-phase dynamics of two other POs with the CO. The points Φ_i^* correspond to in-phase synchronization of two POs with the CO and anti-phase dynamics of the third PO. As in the case of two POs, we are interested in finding the region $\mathcal{A}$ in parameter space, where Φ_i and Φ_i^* are the only attractors (without coexistence of any other stable regimes). This type of dynamics represents different outcomes of the competition between the POs for the synchronization with the CO.

Denote by $\mathcal{A}(\Phi_i)$, $\mathcal{A}(\Phi_i^*)$, $i = 1, 2, 3$, the regions, where the only attractors of the system are Φ_i or Φ_i^*, respectively. As it has been noted, the points Φ_i (and Φ_i^*) are of the same type for $a_1 = a_2 = a_3$, therefore $\mathcal{A}(\Phi_i) \equiv \mathcal{A}(\Phi_j)$, $\mathcal{A}(\Phi_i^*) \equiv \mathcal{A}(\Phi_j^*)$ for any i and j. First we can find the regions $\widetilde{\mathcal{A}}(\Phi_i)$, where any of the points Φ_i or Φ_i^* is stable. These regions are bigger than $\mathcal{A}$ (i.e. $\widetilde{\mathcal{A}}(\Phi_i) \supset \mathcal{A}(\Phi_i)$) since the points Φ_i can coexist with other attractors which are limit or heteroclinic cycles. Then we can find parameter regions and appropriate bifurcations, where unwanted attractors vanish. This usually happens after an Andronov–Hopf bifurcation, pitchfork bifurcation, fold bifurcation of cycles or after the disappearance of heteroclinic cycles through saddle-connection bifurcations. The regions $\mathcal{A}(\Phi_i)$ are marked by b in Fig. 12. The regions $\mathcal{A}(\Phi_i^*)$ are marked by b^* in the same figures.

In the case of different values of a_i, $i = 1, 2, 3$, any of six points Φ_i and Φ_i^* can be the only attractor of the system. Also any coexistence of these points is possible for some parameter values. Thus we have six different regions $\mathcal{A}(\Phi_i)$, $\mathcal{A}(\Phi_i^*)$, $i = 1, 2, 3$, that can intersect with each other. Our aim is to find $\mathcal{A} = \mathcal{A}(\Phi_1) \cup \mathcal{A}(\Phi_2) \cup \mathcal{A}(\Phi_3) \cup \mathcal{A}(\Phi_1^*) \cup \mathcal{A}(\Phi_2^*) \cup \mathcal{A}(\Phi_3^*)$. Each of the mentioned points has its own bifurcation lines (in contrast to the symmetric case) and the problem of finding the proper region becomes more complex.

Here we present two results for the case when the symmetry $a_1 = a_2 = a_3$ is broken.

(1) The regions $\mathcal{A}(\Phi_i)$ and $\mathcal{A}(\Phi_i^*)$ enlarge for parameters p and r when the symmetry of parameters a_i is broken (like in the case $N = 2$).

(2) The region $\mathcal{A}$ enlarges for $a_i \neq a_j$ because new possible cases appear when $\mathcal{A}(\Phi_i) \neq \mathcal{A}(\Phi_j)$ and $\mathcal{A}(\Phi_i^*) \neq \mathcal{A}(\Phi_j^*)$ for $i \neq j$ (this is impossible in the symmetric case).

The region $\mathcal{A}$ is shown in Fig. 17 by grey colour. The figure shows that region $\mathcal{A}$ enlarges when partial symmetry conditions $a_3 = a_1 = 1$ or $a_3 = a_2 = 1.5$ are broken.

5. Discussion

In this paper we presented the results of bifurcation analysis of phase oscillator models with star-like architecture of connections. The case of oscillators with identical natural frequencies was considered. Interaction functions have been described by two terms of Fourier expansion, which makes the dynamical behaviour of the system much more complex than in the case of traditional sinusoid functions. First we derived some general statements about system dynamics identifying its invariant manifolds and symmetries. Then we focused on small systems containing three or four oscillators (one CO + 2 or 3 POs). In terms of phase differences between the CO and POs we have got two or three ODEs that determined the dynamics of the system.

The main results were obtained for parameter space (a, p, r), where a is the universal strength of coupling from POs to the CO, p and r are the parameters of feedforward and feedback interaction functions (without loss of generality the strength of the feedback connection from the CO to POs can be set equal to a constant, e.g. -1). In fact, the detailed bifurcation analysis was performed on the plane (a, r) under different assumptions on p and on the plane (a, p) under different assumptions on r. Then the results were reconsidered and adapted to the case of non-identical connection strengths from POs to the CO (different values of a_i). The case when the dynamics of the system combine in-phase and antiphase oscillations between the CO and POs obtained special attention.

The results of bifurcation analysis are summarized in bifurcation diagrams that provide full description of the boundaries between the regions with different dynamics and the types of bifurcations that lead to the changes in the topology of phase space. These bifurcations include changes of fixed point stability and formation (destruction) of limit and heteroclinic cycles. In 3-dimensional phase space, chaotic behaviour of the model has been investigated. These results are useful to control system dynamics through appropriate choice and variation of parameter values.

The analysis of the system with three oscillators is simple enough to be sure that no bifurcation is missing though we do not have a formal proof of this fact. We did our best to make the list of bifurcations complete also in the case of four oscillators. Still there is a chance that some codimension-two homoclinic type bifurcations are missing. This may happen if their analytical prediction is too difficult.

In the following subsections we try to shed light upon the question to what extent the results obtained can be extended to the systems with more than three POs. Also the comparison with the systems of globally coupled oscillators will be made. Finally some applications to modelling in neurobiology will be discussed.

5.1. Systems with an arbitrary number of peripheral oscillators

As it has been shown, system (1) of $N+1$ coupled oscillators has invariant manifolds (7), (8) of a lower dimension m. The dynamics on these invariant manifolds is the same as for the system that has m POs (in general, the system is not symmetric, that is $f_i \neq f_j$). Therefore any dynamical regime on the invariant manifold will also exist on some invariant manifolds of higher dimensional systems (generally, some additional conditions should be fulfilled). In particular, this implies that the system has chaotic behaviour for some parameter values for any $N \geq 3$. Also, a thorough investigation of stability of the manifold is important because the stability in transversal direction can be different at different parts of the manifold (for example, two dimensional invariant manifolds (14) of system (13) have different types of stability at different points of the manifold).

Further we present some properties of system (3) that together with the properties described in Section 2 give some notion of dynamics in the general N-dimensional case.

Fixed points. System (3) has 2^N fixed points Φ^k that have k coordinates equal to 0 and $N-k$ coordinates equal to π for $k = 0, \ldots, N$ ($O = \Phi^N = (0, \ldots, 0)$, $\Pi = \Phi^0 = (\pi, \ldots, \pi)$). These fixed points are 0-dimensional manifolds of the system and they exist for any odd functions f_j, g that satisfy conditions (2). These points can be the only fixed points of system (3) for some functions and parameter values but additional fixed points can appear for other functions or parameter values (some examples have already been given for $N = 2$ and $N = 3$). The study of basic fixed points is essential for understanding the behaviour of the system. It is possible to analytically investigate the stability of fixed points Φ^k under the parameter variation of the functions $f_i(x)$, $g(x)$. In particular, the stability of the points Φ^k can be studied by computing the eigenvalues of the linearized system.

Local bifurcations and simple dynamical regimes. System (6) has a relatively simple bifurcation structure for $|p| < 1/2$ which includes a series of pitchfork bifurcations of the fixed points O, Π and Φ^k, $k = 1, \ldots, N-1$. The boundaries of surfaces corresponding to these pitchfork bifurcations are marked by a in Fig. 3, Fig. 7 for $N = 2$ and by k in Fig. 12 for $N = 3$; bifurcation lines are marked by $PF(O)$, $PF(\Pi)$, $PF(\Phi)$ in Figs. 3, 7, 9, 12 and 17. We denote by $\mathcal{S}$ the region in parameter space $(a_1, \ldots, a_N, p, r)$ where the system goes through a series of pitchfork bifurcations. The point O is a source in this case, the point Π is a sink, and the system has also $2^N - 2$ other fixed points Φ^k that are saddles. There are no other attractors or repellers except O and Π (a typical example of such dynamics is for the parameter values $a_i = 1$, $b = -1$, $p = r = 0$). Each of these two points undergoes $(N-1)$ pitchfork bifurcations in the transversal direction to the invariant manifold M_1. The hyperplanes of bifurcations are

$$PF^*(O) = \{(a_1, \ldots, a_N, p, r) : p = -1/2\},$$
$$PF^*(\Pi) = \{(a_1, \ldots, a_N, p, r) : p = 1/2\}.$$

Also, each of these fixed points has a pitchfork bifurcation ($PF(O)$ and $PF(\Pi)$, respectively) along the invariant manifold M_1. In general, bifurcation surface of these bifurcations can have a relatively complex structure. In the symmetrical case $a_1 = \cdots = a_N$ the surfaces take the form:

$$PF(O) = \{(a, p, r) : 2p + Na - 2Nar - 1 = 0\},$$
$$PF(\Pi) = \{(a, p, r) : 2p - Na - 2Nar + 1 = 0\}.$$

Two consecutive bifurcations $PF(O)$ and $PF(\Pi)$ keep unchanged the number of fixed points 2^N but transform all points into saddles. In this case the dynamics can be very complex. For example, we can refer to the case $N = 3$ for $a = 1$, $p = r = 0$ where the dynamics is chaotic.

The saddle points $\Phi^k (k = 1, \ldots, N-1)$ can undergo a pitchfork bifurcation and an Andronov–Hopf bifurcation. For each point Φ^k there are two pitchfork bifurcation planes at $p = \pm 1/2$ and two other bifurcation surfaces that correspond to the Andronov–Hopf bifurcation and the pitchfork bifurcation, respectively:

$$AH(\Phi^k) = \{(a, p, r) : 2p - Nar + (k - N/2)a = 0\};$$
$$PF(\Phi^k) = \{(a, p, r) : ((4pr - 2p + 2r - 1)N - 4k(r - p))a - 4p^2 + 1 = 0\}. \quad (19)$$

Thus the region $\mathcal{S}$ is located inside the region $|p| < 1/2$ and is bounded by the surfaces PF and AH. (Note that in general this region consists of a few finite or infinite (relative to the parameters a_i) parts in parameter space $(a_1, \ldots, a_n, p, r)$). The qualitative investigation is easier if it concerns the region $\mathcal{S}$. A cascade of local bifurcations mentioned above creates myriads of new fixed points and limit cycles making the system dynamics very sophisticated.

Other bifurcations. Transcritical bifurcations are also possible in the system. These bifurcations are conditioned by some specific symmetries of the system and can occur along symmetrical invariant manifolds that are transversal to one invariant manifold (usually M_1) (as it has been shown for lower dimensions).

Heteroclinic bifurcations of different types are also typical for the system. We have already mentioned the saddle-connection bifurcation (it is typically accompanied by symmetry breaking), the figure-eight shape homoclinic bifurcation, the saddle–node bifurcation on an invariant curve. There are also bifurcations that create or destroy heteroclinic cycles which are formed by connected separatrices of saddles.

In the symmetric case, the N-dimensional system generates a variety of heteroclinic structures which often disappear with symmetry breaking. Phase space of the system is divided into invariant regions by k-dimensional invariant manifolds (Fig. 10 for $N = 3$) ($k < N$). Disappearance of such invariant manifolds with symmetry breaking is accompanied by bifurcations of the homoclinic tangency type.

System (6) shows interesting and unusual dynamics in the cases of bifurcations of high codimensions. It is possible for simultaneous intersections of many bifurcation surfaces (lines) at the point of maximal codimension in parameter space (Figs. 3, 7, 12 and 17). For example, system (6) has invariant manifolds that intersect at the codimension-3 bifurcation point $(a, p, r) = (1/N, 0, 0)$ for an arbitrary number of oscillators.

Chaos. Starting from the region $\mathcal{S}$, we can formulate necessary (but not sufficient) conditions of chaotic dynamics for $N \geq 3$. First of all, there must be a pitchfork bifurcation of the fixed points O and Π that would transform these points into saddles. The fixed points Φ^k must be saddle-focuses. Other conditions for chaos appearance include the presence of closed heteroclinic structures (such types of structures are shown, for instance, in Fig. 11 for $N = 3$) and intersections of invariant manifolds of the saddles. As it has been shown for $N = 2$ and $N = 3$, many connections between saddles are destroyed when symmetry conditions $a_i = a$ are broken. Partial disappearance of invariant manifolds Q_m for $a_j \neq a_j$ leads to disconnections between different saddles and saddle-focuses which may result in disappearance of chaotic trajectories.

It is difficult to find the lines of bifurcations in a general case because they are mostly codimension-two homoclinic bifurcations and the complete picture of many types of such bifurcations is unknown even in 3D space [24,37]. Another difficulty for the description of chaotic trajectories is that they mostly appear close to a heteroclinic but not homoclinic structure.

Fortunately, the system has also good properties for chaos investigation. The hierarchical structure of the system (described in Section 2.2) can help us understand its dynamics rising from lower-dimensional to higher-dimensional cases. The chaotic structures can be divided into two different categories for each number N of POs. The first one consists of all trajectories that belong to invariant manifolds of dimensions from 3 to $N-1$ and are already studied at previous steps. Therefore the bifurcation diagrams obtained previously are still valid and additional bifurcation surfaces should be considered in the same way. The second case consists of the trajectories that do not belong to any invariant manifold. The bifurcations that lead to this type of chaotic trajectories can be found as bifurcations of heteroclinic structures created from connections of invariant manifolds (as it has been shown for $N = 3$).

The parametric region of chaotic behaviour is bounded by the planes $|p| < 1/2$, $|r| < 1/2$ and pitchfork bifurcations for O, Π, Φ^k. Shilnikov–Hopf type bifurcations [37] are also possible but they are not homoclinic but heteroclinic. Andronov–Hopf bifurcation

surfaces at fixed points Φ^k play a role of boundaries of existence of the chaotic regime. In the symmetrical case, chaos only exists for the values of the parameter $a > 1/N$. This is derived by evaluating local bifurcations at the points O, Π, Φ^k.

Chaotic attractors can coexist with attractors of other types. Such type of multistability is conditioned by the hierarchical structure of the system (see Sections 2.1, 2.2). For example, N-dimensional ($N \geq 4$) system (6) has a chaotic attractor on the manifold M_3 in some parametric region Υ. Suppose that there exists a subregion $\Upsilon_1 \subset \Upsilon$ such that the system has another attractor on the invariant manifold Q_k, $3 \leq k < N$ for parameter values belonging to Υ_1 (this is usually possible as far as the system has an ample quantity of manifolds Q_k for different dimensions k). Then the whole system will be bistable.

Note that the stabilities of the manifolds M_k and Q_k can be different for different points of these manifolds (as it has been shown for the manifolds M_2 for $N = 3$). Therefore a chaotic attractor can leave the manifold if the accuracy of computations is not high enough and the manifold is not completely stable.

If $a_i = a$ and $N \geq 4$, the system always demonstrates multistability of chaotic attractors (if there is at least one). For example, if the system has a chaotic trajectory on the manifold $M_k^{(j)}$, $k \geq 3$, then it has chaotic trajectories on the other manifolds $M_k^{(i)}$, $i \neq j$. Thus starting from the manifold $\varphi_1 = \varphi_2$ and obtaining a chaotic trajectory, we also obtain another chaotic trajectory for initial conditions $\varphi_3 = \varphi_4$. The same situation with multistability takes place for a partially symmetric system when $a_i = a_j \neq a_l$. Since this system has symmetric invariant manifolds, it has multistability of symmetric attractors which can be chaotic.

Finally, it is worth noting that chaos can be one-directional or bi-directional, i.e. for some parameter values the system can have chaotic trajectories when $t \to +\infty$, for other parameter values chaotic trajectories appear when $t \to -\infty$, it may also happen that for some parameter values chaos exists when $t \to \pm\infty$. We described this phenomenon in Section 4 for $N = 3$, but it can be observed for arbitrary N. For example, bi-directional chaos can be found for $(a_1, \ldots, a_N, b, p, r) = (1, \ldots, 1, -1, 0, 0)$, $N > 3$.

5.2. Star-like coupled oscillators versus globally coupled oscillators

The models of *globally* coupled oscillators are well known for a long time and best studied [1,12,20,38–42]. Especially the Kuramoto model of globally coupled phase oscillators is investigated in detail for different types of interaction functions (in particular in the case of equal natural frequencies). The main feature of such type of models is symmetry that implies the existence of invariant manifolds of rather simple forms (straight lines, hyperplanes, etc.). This provides good possibilities for analytical and computational investigations. Any types of models without global coupling usually have more complicated dynamics even in the case when such systems have some sort of symmetries. As an example we can refer to the systems of identical Kuramoto (or Kuramoto–Sakaguchi) oscillators coupled on a ring [43]. Such systems have chimera states for five or more oscillators [44–46].

There are two features of phase oscillator networks that are critical for their complex behaviour: (1) non-global type of coupling, (2) non-identical interaction functions. Each of these conditions is sufficient to obtain chaotic dynamics in a small network. To illustrate this statement, let us consider the following system:

$$\begin{aligned} \dot\theta_0 &= \omega + \sum_{j=1}^{N} f(\theta_j - \theta_0), \\ \dot\theta_i &= \omega + g(\theta_0 - \theta_i) + \sum_{j=1}^{N} h(\theta_j - \theta_i), \quad i = 1, \ldots, N, \end{aligned} \tag{20}$$

where $f(x) = a\sin(x-\alpha)$, $g(x) = b\sin(x-\beta)$, $h(x) = d\sin(x-\delta)$, $a, b, d, \alpha, \beta, \delta$ are the parameters.

For $f(x) = g(x) = h(x)$ the system represents the Kuramoto–Sakaguchi model of globally coupled oscillators. For $h(x) = 0$ we have a star-like coupled system with phase shifts. Consider system (20) with 4 oscillators. If it is a Kuramoto model ($f(x) = g(x) = h(x)$, $\alpha = \beta = \delta = 0$), it cannot have chaotic attractors. As we have shown, a chaotic attractor can appear in the star-like coupled system (without phase shifts) if feedforward and feedback interaction functions are different $f(x) \neq g(x)$. In this case both conditions (1) and (2) are fulfilled. In fact, this is not necessary. For example, it can be shown that chaotic attractors appear in system (20) under the following parameter values: $a = b = 1$, $d = 0$, $\alpha = \beta = \pi/2$; $a = b = 1$, $d = 0.2$, $\alpha = \beta = \delta = \pi/2$; The first set of parameters corresponds to a non-global (star-like coupled) system with identical feedforward and feedback coupling. The second set corresponds to a system with global coupling but non-identical interaction functions. In fact, we can obtain chaos for a wide range of parameters a, b, d and for different values of phase shifts α, β, δ being close to $\pi/2$.

The basic differences between two types of the models mentioned above are in their invariant manifolds. A system of globally coupled oscillators of the Kuramoto-type has invariant manifolds

$$\begin{aligned} \mathcal{P}_m = \{(\theta_0, \ldots, \theta_N) : \theta_0 = \cdots = \theta_{p_1}\,;\, \theta_{p_1+1} = \cdots = \theta_{p_1+p_2}\,; \\ \cdots\,;\, \theta_{\sum_1^{n-1} p_j+1} = \cdots = \theta_N\}, \end{aligned}$$

where $p_1 + p_2 + \cdots + p_m = N$, and

$$\mathcal{M} = \left\{(\theta_0, \ldots, \theta_N) : \sum_{j=0}^{N} e^{i\theta_j} = 0\right\}.$$

The manifolds $\mathcal{P}_m$ correspond to m-cluster states (a partial case of this cluster corresponds to full synchronization $\mathcal{P}_1$) [47]. These manifolds are possible due to permutation symmetry of all oscillators. The second invariant manifold $\mathcal{M}$ is a $(N-1)$-dimensional set in $\mathbb{T}^{N+1}$ that corresponds to the situation when the order parameter of the system is equal to zero [48]. A partial case of the manifold $\mathcal{M}$ is the uniform distribution of oscillator phases around the circle. The manifolds $\mathcal{P}_m$ split the phase space of the system in phase differences into closed identical invariant regions in $\mathbb{R}^N$ [25,48]. Each of these regions consists of a part of the invariant manifold $\mathcal{M}$. Therefore $|\varphi_i| < 2\pi$ and any trajectory cannot intersect the manifold $\mathcal{M}$ if this trajectory does not belong to it. Typical trajectories for the system are symmetric limit and heteroclinic cycles around the manifold $\mathcal{M}$.

The situation is different for star-like coupled system (1). This system has only the permutation symmetry of peripheral oscillators (not all oscillators) and it has the corresponding invariant manifolds M_m that are of a similar type as P_m. System (1) can also have invariant manifolds Q_m for special interaction functions (5) and it does not have $\mathcal{M}$ as an invariant manifold. The invariant manifolds M_m split phase space into invariant regions for the system in phase differences (3). But invariant regions in this case are not bounded in $\mathbb{R}^N$ (phase differences $|\varphi_j - \varphi_j| < 2\pi$, but the variables φ_i are not bounded in contrast to the case of globally coupled oscillators). Limit cycles and quasi-periodic trajectories of (3) in $\mathbb{T}^N$ which are unbounded in $\mathbb{R}^N$ are not possible for the Kuramoto system with global connections.

System (1) has a hierarchical structure relative to its invariant manifolds (8). Adding a new PO to the system with N POs gives a new system which includes the previous system with its invariant manifolds. For example, system (6) with $N+1$ POs and parameters $a_1, \ldots, a_{N-1}, a_N, a_{N+1}$ has the invariant manifold $M_N : \varphi_N = \varphi_{N+1}$ which corresponds to the system of N POs with parameters $a_1, \ldots, a_{N-1}, a_N + a_{N+1}$ (see Section 2.2 for the general case). Such

a feature is absent in the models of globally coupled oscillators. If we add a new oscillator to such a system, the previous system can be considered as an invariant manifold for a new one but the properties of the new and old systems are different. As an example, we can adduce Kuramoto–Sakaguchi model with identical natural frequencies. Consider its m-dimensional invariant manifold that corresponds to the cluster $\theta_i = \theta_j$. The system that represents this manifold loses its permutation symmetry, it does not have its own manifold $\mathcal{M}$ (of a proper dimension) and it does not have heteroclinic cycles when the phase shift parameter is equal to $\pi/2$.

Thus, the system of globally coupled identical oscillators has more symmetries than the system with a star-like coupling and this makes its structure simpler and more convenient for investigation. But hierarchical structure of system (1) provides good possibilities for using the results obtained for lower-dimensional cases for investigation of the higher-dimensional cases. Reduced system (3) is associated with the models of globally coupled phase oscillators considered in the papers [12,17–20]. The study of this system can show new aspects in the study of synchronization of globally coupled models and their applications.

5.3. Biological applications

According to the temporal correlation hypothesis [49] the features of objects that are simultaneously present at the input of sensory systems are coded by synchronous activity of an assembly of neurons representing each object in the brain. The activity of assemblies representing different objects is not synchronous. Following this hypothesis, we assume that the activity in the neocortex can be represented by a system of interacting phase oscillators with each oscillator representing a single external object. We can further simplify the model by assuming that there is no other interaction between the cortical oscillators but through the interaction with the central executive of the attention system that is also represented as a phase oscillator.

This approach has been applied to attention modelling in the papers [50,51] allowing an association of different types of system dynamics with the forms of attention focusing. In particular, the synchronization of the CO with a particular PO was interpreted as focusing attention on the corresponding object. In terms of such a model it is possible to simulate consecutive selection of objects simultaneously present in the visual scene [8] and multiple tracking of moving objects [52].

Another application of phase oscillator networks with the central element is for modelling perception of ambiguous figures. Such a model based on the chaotic dynamics to switch between different perceptions was described in the paper [22]. It has been shown that chaotic dynamics can give the distribution of switching times that coincides with the one observed in psychophysical experiments.

In all these applications a particular set of parameter values and special interaction functions were selected and tested in computational experiments to obtain the necessary behaviour of the system and to satisfy neurobiological data. The present paper provides a general view on the model capabilities allowing the selection of parameters based on the theoretical ground. Moreover, our results can be helpful in organizing a proper evolution of the model dynamics by passing through a predetermined sequence of bifurcations.

The assumption that all natural frequencies of oscillators are identical can be considered as a simplification of the real situation when the range of oscillator frequencies is narrow. In the general case the system should be able to work under arbitrary values of natural frequencies selected in the biologically conditioned frequency range (e.g. gamma frequency range). For non-identical natural frequencies the results obtained are also helpful since they can be used as a starting point for investigation of more complex behaviour associated with this case.

Acknowledgements

We thank Royal Society for a visitor grant enabling O.B. to visit the University of Plymouth for September–November 2010. We also thank P. Ashwin, A. Shilnikov, A. Pikovsky, M. Wolfrum and F. Feudel for useful discussions.

References

[1] Y. Kuramoto, Chemical Oscillations, Waves and Turbulence, Springer-Verlag, Berlin, 1984.
[2] J.A. Acebron, L.L. Bonilla, C.J. Perez Vicente, R. Spigler, The Kuramoto model: a simple paradigm for synchronization phenomena, Rev. Modern Phys. 77 (2005) 137–185.
[3] A. Arenas, A. Diaz-Guilera, J. Kurths, Y. Moreno, C Zhou, Synchronization in complex networks, Phys. Rep. 469 (2008) 93–153.
[4] A. Damasio, The brain binds entities and events by multiregional activation from convergent zones, Neural Comput. 1 (1989) 123–132.
[5] C. Zhou, L. Zemanova, G. Zamora, C.C. Hilgetag, J. Kurths, Hierarchical organization unveiled by functional connectivity in complex brain networks, Phys. Rev. Lett. 97 (2006) 238103.
[6] J. Gómez-Gardeñes, G. Zamora-López, Y. Moreno, A. Arenas, From modular to centralized organization of synchronization in functional areas of the cat cerebral cortex, PLoS ONE 5 (8) (2010) e12313.
[7] G. Zamora-López, C. Zhou, J. Kurths, Cortical hubs form a module for multisensory integration on top of the hierarchy of cortical networks, Frontiers Neuroinform. 4 (2010) http://dx.doi.org/10.3389/neuro.11.001.2010.
[8] R. Borisyuk, Y. Kazanovich, Oscillatory model of attention-guided object selection and novelty detection, Neural Netw. 17 (2004) 899–915.
[9] D. Chik, R. Borisyuk, Y. Kazanovich, Selective attention model with spiking elements, Neural Netw. 22 (2009) 890–900.
[10] A. Baddeley, Exploring the central executive, Q. J. Exp. Psychol. 49A (1996) 5–28.
[11] G.G. Gregoriou, S.J. Gotts, H. Zhou, R. Desimone, High-frequency, long-range coupling between prefrontal and visual cortex during attention, Science 324 (2009) 1207–1210.
[12] D. Golomb, D. Hansel, B. Shraiman, H. Sompolinsky, Clustering in globally coupled phase oscillators, Phys. Rev. A 45 (1992) 3516–3530.
[13] D. Huang, G. Pipa, Achieving synchronization of networks by an auxiliary hub, EPL 77 (2007) 50010.
[14] Y. Kazanovich, R. Borisyuk, Synchronization in oscillator systems with a central element and phase shifts, Progr. Theor. Phys. 110 (2003) 1047–1058.
[15] I. Omelchenko, Yu. Maistrenko, E. Mosekilde, Synchronization in ensembles of coupled maps with a major element, Discrete Dyn. Nat. Soc. (2005) 239–255.
[16] F. Sorrentino, M. di Bernardo, G. Huerta Cuellar, S. Boccaletti, Synchronization in weighted scale free networks with degree–degree correlation, Physica D 224 (2006) 123–129.
[17] A. Marvel, R.E. Mirollo, S.H. Strogatz, Identical phase oscillators with global sinusoidal coupling evolve by Möbius group action, Chaos 19 (2009) 043104.
[18] J.W. Swift, S.H. Strogatz, K. Wiesenfeld, Averaging of globally coupled oscillators, Physica D 55 (1992) 239–250.
[19] K.Y. Tsang, R.E. Mirollo, S.H. Strogatz, K. Wiesenfeld, Dynamics of a globally coupled oscillator array, Physica D 48 (1991) 102–122.
[20] S. Watanabe, S.H. Strogatz, Constants of motion for superconducting Josephson arrays, Physica D 74 (1994) 197–253.
[21] H. Kitajima, J. Kurths, Bifurcation in neuronal networks with hub structure, Physica A 388 (2009) 4499–4508.
[22] R. Borisyuk, D. Chik, Y. Kazanovich, Visual perception of ambiguous figures: synchronization based neural models, Biol. Cybern 100 (2009) 491–504.
[23] Yu.A. Kuznetsov, Elements of Applied Bifurcation Theory, Springer-Verlag, New York, 2004.
[24] L.P. Shilnikov, A.L. Shilnikov, D. Turaev, L.O. Chua, Methods of Qualitative Theory in Nonlinear Dynamics, vols. 1 and 2, World Scientific, Singapore, 1998, 2001.
[25] P. Ashwin, J.W. Swift, The dynamics of n weakly coupled identical oscillators, J. Nonlinear Sci. 2 (1992) 69–108.
[26] V.I. Arnold, The evolution of a magnetic field under the influence of transport and diffusion, in: V.M. Tikhomirov (Ed.), Some Questions of Present-Day Analysis, Moscow University, 1984 (in Russian).
[27] J.K. Hale, H. Koçak, Dynamics and Bifurcations, Springer-Verlag, New York, 1991.
[28] V.I. Arnold, Sur la topologie des équolements stationnaires des fluides parfaits, C. R. Acad. Sci. Paris 261 (1965) 17–20.
[29] P. Ashwin, O. Podvigina, Hopf bifurcation with cubic symmetry and instability of ABC flow, Proc. R. Soc. Lond. A 459 (2003) 1801–1827.
[30] S. Childress, New solutions of the kinematic dynamo problem, J. Math. Phys. 1 (1970) 3063–3076.
[31] T. Dombre, U. Frisch, J.M. Greene, M. Hénon, A. Mehr, A.M. Soward, Chaotic streamlines in the ABC flows, J. Fluid Mech. 167 (1986) 353–391.
[32] F. Feudel, N. Seehafer, B. Galanti, S. Rüdiger, Symmetry-breaking bifurcations for the magnetohydrodynamic equations with helical forcing, Phys. Rev. E 54 (1996) 2589–2596.
[33] D. Galloway, U. Frisch, A note on the stability of a family of space-periodic Beltrami flows, J. Fluid Mech. 180 (1987) 557–564.

[34] M. Henon, Sur la topologie des lignes de courant dans un cas particulier, C.R. Acad. Sci. Paris A 262 (1966) 312–314.
[35] O. Podvigina, A. Pouquet, On the non-linear stability of the 1:1:1 ABC flow, Physica D 75 (1994) 471–508.
[36] S. Childress, A.M. Soward, On the rapid generation of magnetic field, in: J.R. Buchler (Ed.), Chaos in Astrophysics, Kluwer, Dordrecht, 1985, pp. 233–244.
[37] A.R. Champneys, Yu.A. Kuznetsov, Numerical detection and continuation of codimension-two homoclinic bifurcations, Int. J. Bifurcation and Chaos 4 (1994) 785–822.
[38] H. Daido, Onset of cooperative entrainment in limit-cycle oscillators with uniform all-to-all interactions: bifurcation of the order function, Physica D 91 (1996) 24–66.
[39] D. Hansel, G. Mato, C. Meunier, Clustering and slow switching in globally coupled phase oscillators, Phys. Rev. E 48 (1993) 3470–3477.
[40] A. Pikovsky, M. Rosenblum, J. Kurths, Synchronization. A Universal Concept in Nonlinear Sciences, Cambridge University Press, Cambridge, 2001.
[41] H. Sakaguchi, Y. Kuramoto, A soluble active rotator model showing phase transition via mutual entrainment, Progr. Theoret. Phys. 76 (3) (1986) 576–581.
[42] S.H. Strogatz, From Kuramoto to Crawford: exploring the onset of synchronization in populations of coupled oscillators, Physica D 143 (2000) 1–20.
[43] D.A. Wiley, S.H. Strogatz, M. Girvan, The size of the sinc basin, Chaos 16 (2006) 015103.
[44] D.M. Abrams, S.H. Strogatz, Chimera states for coupled oscillators, Phys. Rev. Lett. 93 (2004) 174102.
[45] A.E. Motter, Nonlinear dynamics: spontaneous synchrony breaking, Nature Physics 6 (2010) 164–165.
[46] O. Omel'chenko, M. Wolfrum, Yu. Maistrenko, Chimera states as chaotic spatiotemporal patterns, Phys. Rev. E 81 (2010) 065201.
[47] O. Burylko, A. Pikovsky, Desynchronization transitions in nonlinearly coupled phase oscillators, Physica D 240 (2011) 1352–1361.
[48] P. Ashwin, O. Burylko, Y. Maistrenko, Bifurcation to heteroclinic cycles and sensitivity in three and four coupled phase oscillators, Physica D 237 (2008) 454–466.
[49] W. Singer, C.M. Gray, Visual feature integration and the temporal correlation hypothesis, Ann. Rev. Neurosci. 18 (1995) 555–586.
[50] Y. Kazanovich, R. Borisyuk, Synchronization in a neural network of phase oscillators with the central element, Biol. Cybern. 71 (1994) 177–185.
[51] Y. Kazanovich, R. Borisyuk, Dynamics of neural networks with a central element, Neural Networks 12 (1999) 1441–1454.
[52] Y. Kazanovich, R. Borisyuk, An oscillatory neural model of multiple object tracking, Neural Comput. 18 (2006) 1413–1440.